AD-A224 846

TECHNICAL REPORT

For the period: Oct. 1, 1989 - Sept. 30, 1990
Under Contract No. : N00014-89-J-1267 (10/1/88 - 9/30/90)

Li – SF_6 COMBUSTION IN STORED CHEMICAL ENERGY PROPULSION SYSTEMS

S.H. Chan, C.C. Tan, Y.G. Zhao and P.J. Janke

Prepared for the Department of the Navy
Office of Naval Research
Arlington, VA 22217

UWM™

Department of Mechanical Engineering
University of Wisconsin--Milwaukee
P.O. Box 784
Milwaukee, Wisconsin 53201
July 1, 1990

$Li - SF_6$ COMBUSTION IN STORED CHEMICAL ENERGY PROPULSION SYSTEMS

S.H.Chan[1], C.C.Tan[2], Y.G.Zhao[2] and P.J.Janke[2]

Department of Mechanical Engineering

University of Wisconsin—Milwaukee

P.O.Box 784, Milwaukee, Wisconsin 53201

TECHNICAL REPORT

Prepared for the Department of Navy

Office of Naval Research

Arlington, VA 22217

Under Contracts No.: N00014-89-J-1267

For the Period: Oct. 1, 1989 — Sept. 30, 1990

July 1, 1990

---

1 Wisconsin Distinguished Professor

2 Graduate Research Assistant

TABLE OF CONTENTS

ABSTRACT

Appropriate thermodynamic models and thermo-chemical data for multicomponents and immiscible phases have been incorporated into a code for the computation of chemical equilibrium of the reactants used in a stored chemical energy propulsion system. The reactants considered are molten lithium fuel and gaseous sulfur hexafluoride oxidant. Extensive equilibrium state relationships as a function of mixture fraction have been presented over a temperature range of possible operating conditions. They were subsequently employed to predict the complex flow structure of a choked, turbulent, reacting SF_6 gas jet submerged in a molten lithium bath. Detailed profiles of velocity, temperature, void fraction and mass fraction of all phases in the jet have been presented. The results show that the reaction is completed within a short distance from the injector but the plume jet penetrates farther beyond due to significant evaporation of lithium fuel in the hot temperature plume, and subsequent condensation of the evaporated fuel and reaction products in the later part of the plume. The effect of lithium subcooling on flow structure has also been examined. It is found that lowering the degree of subcooling by raising the fuel bath temperature increases fuel evaporation, decreases the entrainment rate, delays the completion of reaction and lengthens greatly the jet penetration distance. Finally, for practical use, a simple correlation of the jet penetration length as a function of subcooling has also been presented.

ACKNOWLEDGEMENT

This research was sponsored by the U.S. Office of Naval Research, Grant No. N00014-89-J-1267, under the technical management of Dr. G. Roy.

STATEMENT "A" per Dr. Gabriel Roy
ONR/Code 1132P
TELECON 7/27/90 VG

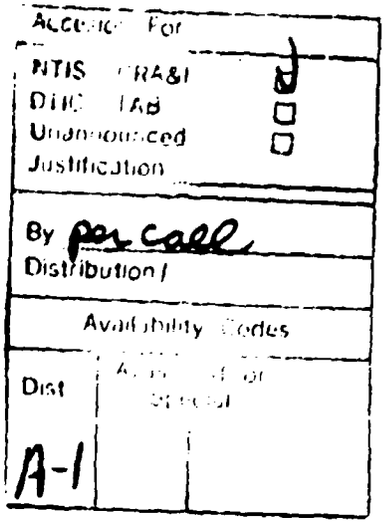

LIST OF TABLES

LIST OF FIGURES

NOMENCLATURE

A'_{ij}	interpreted as interaction energy
b_i	quasi-lattice parameters
C_p	specific heat
D	injector diameter
f	mixture fraction
g	the square of mixture fraction fluctuation
ΔH_r	heat of reaction
K	turbulent kinetic energy
L	plume length
N_i	moles of chemical species i
R	gas constant
T	Temperature
u	axial velocity
X	axial distance
Y	mass fraction

Greek Symbols

γ_k	activity coefficient of kth species
ρ	density
ϵ	turbulent dissipation rate

Superscripts

~	Favre averaged quantities
-	time averaged quantities

Subscripts

k	k species
0	jet nozzle condition
∞	bath (or surrounding) condition
S	solid
L	liquid
G	gas
d	down stream
u	up stream

1. INTRODUCTION

After an extended period of study,[1-5] the closed Rankine-cycle, lithium fueled SCEPS (Stored Chemical Energy Propulsion System) has emerged as the best choice for undersea propulsion system.[6-7] The SCEPS derives its chemical heat source from the highly exothermic reaction between an alkali liquid metal fuel and a halogen gas oxidant. The reactants are so selected to yield several advantages and unique features for underwater propulsion. First, the energy density value is exceptionally high on a total reactants (fuel plus oxidant) gravimetric basis. Secondly, the products of combustion are in condensed (liquid and solid) phases and their combined density is greater than the density of molten fuel. These characteristics permit the use of a closed reactor for a near-constant volume, bath-type combustion process. Furthermore, the reactor initially holding the molten metal fuel will become the holding tank to house combustion products and no discharge of products from the reactor to the environment is necessary. Coupling this thermal energy source reactor to a closed Rankine steam cycle to propel a turbine, the performance of such a combined power system is therefore insensitive to operating depth, making it well suited for undersea applications.

Among reactants for undersea propulsion, the use of lithium (Li) fuel with sulfur hexafluoride (SF_6) oxidant appears to be the best candidate for the SCEPS concept. They are relatively economical. The SF_6 oxidant is inert and non-toxic. The heat of reaction based on a unit mass of total reactants exceeds even that of H_2/O_2 reactants.[1] They are being adopted for the on-going SCEPS project. However, to the authors' best knowledge, the flow structure analysis of turbulent SF_6 gas jets submerged in and reacting with a molten lithium has not been reported in the literature.

Prior work on the related subject is very limited. A Na/Cl system was analyzed by a simplified integral model[8] which was improved[9] by the use of the local homogeneous flow approximation, equilibrium combustion model and κ-ϵ-g model.[10] The predictions seem to agree with the data of a highly diluted, non-evaporating sodium fuel.[8] Later it was incorporated into the model a general scheme for complex equilibrium computation for nonideal multiphase electrolytic system,[11] which was tested successfully with the data[12] of a reacting, evaporating and condensing system--HCl/aqueous ammonia solution containing up to 25% of $NH_{3(aq)}$ to simulate the metal fuel.

This study draws from the prior works[9,11] and extends to Li/SF_6 system. Specifically, the thermodynamic properties of the multiphase, nonideal reacting mixture of $Li_{(L)}/SF_{6(g)}$ reactants in chemical equilibrium are constructed and presented as a function of mixture fraction (state relationships). They are then used to predict the turbulent flame structure of Li/SF_6 reacting jets. The former provides the fundamental information useful for combustion studies in general while the latter predicts the detailed flow structure of the complex flame-like jets which may contain several liquid and solid phases due to partial miscibility of molten lithium fuel and its reaction salt product, lithium fluoride.

2. EQUILIBRIUM STATE RELATIONSHIPS

2.1 Formulation

The information on equilibrium state relationships are prerequisite to the analysis of the flame structure of a SF_6 gas jet reacting in a molten Li fuel. The required relationships include equilibrium compositions of all species in all phases, the equilibrium temperature and density of the mixture resulting from the reaction of molten Li with gaseous SF_6 at various mixture fractions.

The general formulation for the state relationships has been described earlier.[9,11] Briefly, it utilizes a variation of the direct Gibbs free energy minimization approach. The minimization is subject to element abundance and charge balance constraints. A general purpose code was developed for complex equilibrium computation for nonideal multiphase systems (CEC-NMS), which has been extensively tested[11,13] for a simulant reactant pair of HCl as oxidant and aqueous ammonia solution as fuel to confirm the validity of the overall approach.

One of the objectives in the present study is to include in the code the specific thermodynamic models and the necessary thermo-chemical property data of the SF_6-Li reacting system and then perform the complex equilibrium computation of the SF_6 and Li reactants for SCEPS.

2.2 Li-SF_6 Reaction System

The stoichiometric reaction between lithium and sulfur hexafluoride can be expressed as[3]

$$8\ Li + SF_6 \rightarrow 6\ LiF + Li_2S$$

which liberates a large amount of thermal energy and produces lithium fluoride, the dominant product, and lithium sulfide, the minor product. For generality, whether the reaction is stoichiometric or not, the gas phase of the reacting mixture in the present study allows for the possible existence of fifteen species. They are Li, Li_2, F, F_2, LiF, Li_2F_2, Li_3F_3, SF, SF_2, SF_4, SF_6, S_2F_2, Li_2S, S and S_2, which are assumed to behave as an ideal gas mixture. Four solid species are considered in separate phases: $Li_{(s)}$, $LiF_{(s)}$, $S_{(s)}$ and $Li_2S_{(s)}$.

The liquid phase is assumed to contain three possible species: $Li_{(L)}$, $LiF_{(L)}$ and $Li_2S_{(L)}$. The liquid metal, $Li_{(L)}$, and the molten salt, $LiF_{(L)}$, can form two immiscible phases with an additional component, $Li_2S_{(L)}$, dissolved

in each phase to form ternary mixtures. The activity coefficients of the immiscible liquid phases (metal-rich phase (L-1) and salt-rich phase (L-2)) are predicted using the multicomponent van Laar model.[14] The activity coefficient of the kth species may be given as

$$\ln \gamma_k = b_k \sum_i \sum_j (A'_{ik} - 0.5A'_{ij})\, b_i b_j N_i N_j / [RT\, (\sum_i N_i b_i)^2] \qquad (1)$$

where A'_{ij} and b_i are empirical parameters. Note that $A'_{ii} = 0$, and $A'_{ij} = A'_{ji}$. The equation given here differs from that presented by Groff and Faeth (ref. 15, p. 22, and ref. 16, p. 328). We believe this equation to be the correct one.

For a system with three components, the number of empirical parameters may be reduced by one by defining new parameters A_{ij} and B_i as[15]:

$$A_{ij} = b_i A'_{ij}; \quad B_1 = b_1/b_2; \quad B_2 = b_2/b_3; \quad \text{and } B_3 = b_1/b_3 = B_1 B_2 \qquad (2)$$

The subscripts 1, 2, and 3 refer to $Li_{(L)}$, $LiF_{(L)}$, and $Li_2S_{(L)}$, respectively. Equation (1) may then be written as

$$\text{Ln } \gamma_k = \sum_i \sum_j (A_{ik} - 0.5A_{ij})\, (b_j/b_k)\, N_i N_j / RT\, [\sum_i N_i\, (b_i/b_k)]^2 \qquad (3)$$

The estimated empirical parameters, A_{ij}, from experimental data in units of (kJ/mole) are a function of temperature (K) as,[15]

$$A_{12} = 121.53 - 0.05730\ T; \quad A_{13} = 53.287 - 4.00E\text{-}4\ T; \quad A_{23} = 0 \qquad (4)$$

$$B_1 = 2.5846 - 8.132E\text{-}4\ T; \quad B_3 = 1.36; \quad B_2 = B_3/B_1 \qquad (5)$$

2.3 Thermodynamic Data

Thermodynamic data for all three forms of Li_2S is extremely limited. Groff and Faeth[15] estimated the required spectroscopic data for determining

the properties of $Li_2S_{(g)}$ using statistical methods. They felt the accuracy of the resulting thermodynamic data for $Li_2S_{(g)}$ to be within ± 5%. Their equations are used in this work to calculate the enthalpy and Gibbs energy of gaseous lithium sulfide. They also estimated thermodynamic data for $Li_2S_{(s)}$ and $Li_2S_{(L)}$ from Na_2S, Li_2O, and Na_2O using Kopp's rule.[17] Their estimated values were used to calculate the enthalpy and Gibbs energy for solid and liquid lithium sulfide. The thermodynamic data for all other species were taken from the data file provided with the CEC-72 computer program.[18]

2.4 Comparison with Experimental Data

The equilibrium results to be presented later involve a multiphase and multi-species system. No experimental data is available to compare these results to, nor have any calculations of this type appeared in the literature. It is decided to test the validity of the above thermodynamic model and the accuracy of the numerical calculations by computing the phase equilibrium diagrams of binary systems of which experimental data are available for comparison. The tests include Li-Li_2S, Li-LiF, and LiF-Li_2S binary systems. A representative comparison between the prediction (indicated by dots) and experimental data[16,19] (line) of the Li-Li_2S binary is shown in Fig. 1. Good agreement was found in all binaries.

2.5 Equilibrium Results

The above thermodynamic model and data have been properly incorporated into CEC-NMS code to calculate equilibrium state relationships. As stated above, the resulting code has been tested against the binary data and is now ready for multi-species computations. The equilibrium results are presented in Figs. 3 to 6 for the reaction of a gaseous SF_6 at T_o = 298 K with a

molten Li at T_∞ = 1130 K, 1358 K, 1415 K, 1586 K, respectively and one atmosphere pressure.

Figure 3 to 6 show the equilibrium temperature, density, void fraction, mass fractions of gas, liquid and solid phases as a function of mixture fraction f. The latter is so defined that f = 1 designates the pure SF_6 gas and f = 0 indicates the pure molten Li metal. In Figs. 7 to 34 the corresponding mass fractions of all individual species in each of three phases are provided. By referring to Figs. 3 to 6, as the value of f in the reacting system decreases from one, the equilibrium temperature increases while the mixture density decreases. However, the temperature is still low enough that a condensed solid phase of $LiF_{(s)}$ emerges in a narrow range and another condensed liquid phase of $LiF_{(L)}$ also appears in a narrow range, which can be verified by checking Figs. 11 to 14. The co-existed gas phase is composed of the excess SF_6 gas and vapors of combustion products. As f decreases to the stoichiometric value of f_{st} = 0.72, where temperature reaches the maximum and density the minimum, all species are turned into gaseous/vapor phase. Further decreasing in f will result in a lower temperature, higher density and the appearance of a liquid phase. Since molten Li and LiF liquids are partially immiscible, which is accounted for in the present formulation, one might expect co-existence of two liquids: metal rich phase (L-1) and salt-rich phase (L-2). However our equilibrium results reveal only one liquid in existence at a time. This can be explained as follows.

The necessary condition for two liquids to co-exist is that the mixture is fuel-rich, i.e., when $0 < f < f_{st}$. However in most of region in f = 0 to f_{st}, the mixture equilibrium temperature exceeds the consolute temperature (1600 K), the maximum temperature above which two immiscible liquids can not co-exist. Naturally, only single liquid exists. For the rest of the region,

LiF is below the solubility limit so that again only one liquid exists. A clear picture can be seen by referring to the Li-LiF phase diagram[16,19] shown in Fig. 2. The equilibrium states in the present study all lie in the one liquid region above the two-liquid dome. For this reason, the computer printouts do not discern (L-1) liquid from (L-2) liquid and similar species are lumped together. For example, in Figs. 23 to 26, the liquid lithium fuel species is then indicated by $(Li_{(L-1)} + Li_{(L-2)})$ or $(Li_{(L-1)})$, and so forth.

From the results of the current equilibrium state relationships, one can expect that no two immiscible liquids will co-exist in the reacting plume to be studied in the later section. However, it does not preclude the two immiscible liquids from forming outside the plume region when the mixture temperature drops because of heat losses to surrounding heat exchangers.

It is interesting to point out that for the identical initial oxidant temperature of 298 K and the fuel temperature of 1130 K, an immiscible liquid region does appear in sodium-chlorine reacting system,[9] but not in the present lithium-sulfur hexafluoride system. Had the initial bath temperature of lithium been lower, it is likely that the solubility limit of the salt in the metal would have been reached at a lower temperature. Then the salt-rich liquid would begin to form at a temperature below the consolute temperature and an immiscible liquid region would appear.

Similar equilibrium results have been obtained for lithium fuel maintained at four elevated temperatures listed in Table 1. They will be used later in the study of subcooling effects on the flow structure of SF_6 jets reacting in molten Li pools.

3. STRUCTURE OF SF_6 JETS IN MOLTEN Li

3.1 Mathematical Model

The combustor under consideration is a large vessel filled with a molten Li fuel at one atmospheric pressure. A gaseous oxidant SF_6 drawn from a liquefied storage tank, is discharged into a large vessel through a small injector mounted at the bottom of the vessel. The choked, turbulent SF_6 gas jet will react with the entrained molten Li to form a complex, multiphase, axisymmetric jet. A steady jet is the subject under investigation. In practice, the fuel vessel is finite in size and the reaction is transient in nature. The current steady state calculation provides results at a given time. With the state relationships developed above, the structure of the steady reacting jet is to be predicted. The flow model adopted here follows closely the method developed previously.[9,10] Basically, it employs the local homogeneous two-phase flow model, the local chemically equilibrium combustion model with the foregoing equilibrium state relations, and Shvab-Zeldovich type of formulation. The conserved equations to be solved are summarized in the previous papers[9,11] and will not be re-iterated here. They include the Favre-averaged parabolic form of transport equations for continuity, momentum, mixture fraction ($\tilde{f}$), turbulence kinetic energy (k), the rate of turbulence dissipation (ε) and the square of the mixture fraction fluctuation (g). The mean scalar properties other than those from the solu- tion of transport equations are determined locally in the plume by integrating the product of the corresponding equilibrium state relationships and a clipped Gaussian probability density profile over the entire range of the mixture fraction.

3.2 Comparison with Experimental Data

Again as in the state relationships, no experimental data nor numerical calculations are available for comparison with the flow structures of Li-SF_6 system to be presented next. However, the above mathematical model and the resulting modified GENMIX code developed in this laboratory were extensively tested using experimental data[12] of metal simulant reactants (HCl-NH_3 aqueous solution) in our recent studies[11,13] Good agreement was found between predictions and data for various fuel temperature, pressure and concentration conditions. The primary purpose of those studies is in fact to lay a ground work for the present liquid metal combustion study, the results of which are given below.

3.3 Li-SF_6 Flow Structure

The initial condition of the sulfur hexafluoride gas jet at the injector exit is assumed to be uniform and taken as[11,13]

$$\rho_o = 5.97 \text{ Kg/m}^3, \qquad T_o = 298 \text{ K}, \qquad \tilde{u}_o = 203.4 \text{ m/s}$$

$$\tilde{f}_o = 1, \qquad k_o = (0.03\ \tilde{u}_o)^2, \qquad \varepsilon_o = (0.03\ \tilde{u}_o)^3/D, \qquad g_o = 0 \tag{6}$$

The injector diameter $D = 7.9 \times 10^{-4}$ m is used in the computation. At the plume center axis, the radial gradients of $\tilde{u}$, $\tilde{f}$, k, ε, and g are set to zero due to symmetry. At the outer boundary of the jet, $g = 0$, $\tilde{u} = 0.0005\ u_o$ and $\tilde{f} = 0.0005\ \tilde{f}_o$ are assumed, while k and ε are described by $k = (0.03\ \tilde{u}_o)^2$, and $\varepsilon = (0.03\ \tilde{u}_o)^3/D$ at the first axial step. At later steps on the outer boundary,

$$k_d = k_u - \varepsilon_u\ \Delta x/\tilde{u}_u; \quad \varepsilon_d = \varepsilon_u - C_{\varepsilon 2}\ \varepsilon_u^2\ \Delta x/(k_u\ \tilde{u}_u) \tag{7}$$

which are obtained by solving the governing equations with the radial convective and diffusive terms neglected. The subscripts d and u denote the downstream and upstream points, respectively. The numerical computational details are given in the previous study.[11]

Using the above initial and boundary conditions, and incorporating the equilibrium state relationships in the modified GENMIX code, the structure of a reacting SF_6 gas jet submerged in a molten lithium bath has been computed. Figs.35-38shows the predicted mean quantities along the center axis of the jet when the bath temperature is maintained separately at T_∞ = 1130 K and etc. , in which 1 atm. pressure is maintained. Centerline velocity ($\tilde{u}/\tilde{u}_o$), mixture fraction ($\tilde{f}$), temperature ($\tilde{T}$), gas mass fraction ($\tilde{Y}_g$), liquid mass fraction ($\tilde{Y}_L$), solid mass fraction ($\tilde{Y}_s$) and void fraction ($\tilde{\alpha}$) are plotted against the dimensionless distance (x/D) from the injector exit. It is seen that the mixture temperature rises sharply in a narrow range of (x/D). Combustion products appear in solid and liquid phases with some overlapping near the injector due to relatively low mixture temperature. Then they turn into vapor phase around the high temperature zone and finally into liquid phase far away from the injector. The complete condensation of reaction products is one of the unique and desirable features of the SCEPS, which results in a relatively short plume length of L/D = 5.6. The plume length here is arbitrarily taken as the length where the void fraction reduces to 0.01. It is the total length which includes the reaction, evaporation and condensation regions. The flow structure computation indicates that the reaction region ends at x/D = 3.9 where the injected SF_6 oxidant is consumed almost completely (the mean mass fraction of SF_6 and all its derivatives like dissociated elements etc. reduces, say, to 0.001 along the jet axis). As the mixture temperature increases in the reaction region the evaporation of the molten Li entrained

into the jet stream from the surrounding bath becomes increasingly important. The excess evaporated fuel and combustion products are eventually condensed downstream. This evaporation-condensation region partially overlaps with the reaction region; its length is rather substantial and cannot be ignored. Further checking of species presented in the evaporation-condensation region indicates that the lithium fuel vapor outweighs the reaction product vapor. This can be explained if reference is made to the equilibrium composition in Figs. 11 to 14. Analogous to the flow structure diagram, the corresponding reaction region in Figs. 11 to 14 is approximately extended from f = 1 to 0.67 at which the oxidant SF_6 gas and its derivative components are practically all consumed in the reaction. Similarly the evaporation-condensation region lies between f = 0.79 to 0.13. It is clearly seen that in some evaporation-condensation region the mass fraction of fuel ($Li + Li_2$) vapor, indeed far exceeds that of the vapor product ($LiF + Li_2F_2 + Li_3F_3$).

3.4 Subcooling Effect

To investigate effects of subcooling on turbulent structure of reacting jets, the bath fuel temperature is varied from 1130 K to 1586 K as shown in Table 1. It covers practically all the possible operation range of SCEPS. Since the working temperature of the reactor must be so chosen that the reaction products are in liquid state, the lowest possible operation temperature is limited by the melting point of the mixture of lithium fluoride and lithium sulfide, which is 1083 K. Similarly, the maximum temperature is bounded by the saturation (boiling) temperature of lithium fuel, which is 1609 K.

Flow structures of all subcooling cases listed in Table 1 have been computed. Figures 35 to 38 show the effect of subcooling on the plume penetration. When the bath temperature is increased from 1130 to 1586 K, the

.oling temperature (i.e. saturation temperature minus bath temperature) is reduced from 479 K to 23 K (minimum subcooling), and the plume penetration length is also increased in an order of magnitude. In fact the reduction in fuel subcooling delays considerably the appearance of solid and liquid phases. Also delayed is the temperature peak which implies that the primary reaction occurs at further downstream from the injector. The latter is attributed to the reduction in the fuel entrainment rate in spite of increasing fuel evaporation. Since Li vapor is lighter than the Li liquid in the bath and SF_6 gas in the main jet stream, the jet mixture density decreases near the boundary as more Li evaporates from the jet interphase boundary. Consequently the turbulent viscosity and the entrainment rate of the ambient fuel are reduced accord- ingly. Similar phenomenon has been observed in the simulant reactant pair of hydrogen chloride gas reacting with ammonia solution.[11]

3.5 Plume Length Correlation

The total penetration length is one of the key parameters needed for the design of the liquid metal combustor. It is desirable if the plume lengths from the above complex computation can be correlated by a simple equation for practical use.

With the consideration of a simple entrainment expression and the energy balance between the reaction heat release and heating and vaporization of the entrained fuel, the plume length could be grossly estimated as[12]

$$\frac{L}{D} = c \frac{\Delta H_r}{c_p \Delta T} \left(\frac{\rho_o}{\rho_\infty}\right)^{1/2} \tag{8}$$

where c is a correlation constant, ΔH_r is the heat of reaction per unit mass of oxidant, c_p is the specific heat of the bath liquid and ΔT is the

degree of subcooling of the bath liquid. Table 1 lists most of the relevant parameters including the computed plume lengths under various subcooling conditions. The L in the above equation represents the length over which all the reaction heat is dissipated by the sensible heat of the entrained liquid from the bath. It is consistent with the notion that the plume mostly consists of fuel vapor produced by reaction heat release and that the plume length is determined by the distance required for the condensation of the fuel vapor. The equation is essentially identical to the correlation of Weimer et al.[20] for their data on penetration lengths of condensing vapor jets in liquids. The c value proposed by Weimer et al.[20] is 17.8 which was also used for Na-Cl_2 system.[8,12] For HCl-NH_3 aqueous solution system, about half of that value was suggested.[12] In the present Li-SF_6 reacting system, we attempt to correlate the subcooling effect by equation (8). The value of the correlation constant is found to be 5.506 by the least square method. The absolute deviation in the plume length of the correlation from the computed length is between 1.8 to 57%.

4. CONCLUSIONS

The liquid metal combustion in stored chemical energy propulsion system has been analyzed. The necessary thermodynamic data have been presented and incorporated into a general purpose code to account for nonideal solutions forming immiscible phases. Specifically, equilibrium state relationships of the gaseous SF_6-molten Li reacting system have been presented as a function of mixture fraction. Comparisons have been made with limited experimental data available and good agreement is found. Using the state relationships and appropriate flow models, the structure of sonic, turbulent, reacting SF_6 gas jets submerged in molten Li baths has been obtained. Velocity, temperature,

void fraction, and mass fractions of gas, liquid and solid phases, etc. in the reacting jets have been presented. The plume length is found to be finite, due to condensation of reaction products, but penetrates far beyond the reaction length because the lithium fuel evaporated in the high temperature region must be re-condensed in lower temperature region. The subcooling effect has also been examined and found to greatly affect the flow structure by shifting the structure downstream when the degree of subcooling is reduced. Finally a simple equation is presented which correlates the plume length as a function of subcooling satisfactorily. The results of the present study make possible the prediction of flow structure in the current design of SCEPS for undersea propulsion systems.

REFERENCES

1. Myers, P. S.: SAE National Powerplant Meeting, Paper 690304, Oct. 27-29 (1969).

2. Mattavi, J. N., Heffner, F. E., and Miklos, A. A.: SAE Transactions 78, 2376 (1969).

3. Biermann, U. K. P.: Proc. of Tenth Intersociety Energy Conf., 1023 (1975).

4. Van der Sluys, W. L. N.: Proc. of Tenth Intersociety Energy Conf., 1031 (1975).

5. Groff, E. G. and Faeth, G. M.: J. Hydronautics 12, 63 (1978).

6. Bush, K. L. and Merill, G. L.: AIAA/SAE/ASME 17th Joint Propulsion Conference, July 27-29 (1981).

7. Hughes, T. G., Smith, R. B., and Kiley, D. H.: J. Energy 7, 128 (1983).

8. Avery, J. F. and Faeth, G. M.: Fifteenth Symp. (Intl.) on Combustion, The Combustion Institute, Pittsburgh, 501 (1975).

9. Chen, L. D. and Faeth, G. M.: Comb. Sci. Tech. 11, 111 (1983).

10. Lockwood, F. C. and Naguib, A. S.: Comb. Flame 24, 109 (1975).

11. Chan, S. H., Janke, P. J., and Shen, T. R.: Twenty-second Symposium (International) on Combustion, The Combustion Institute, 721 (1988).

12. Cho, D. H., Armstrong, D. R. and Bova, L.: ASME Proceedings of the National Heat Transfer Conf. 1, 27 (1988).

13. Chan, S. H. and Shen, T. R.: Heat Transfer Phenomena in Radiation, Combustion and Fires, HTD-Vol 106, ASME/AIChE National Heat Transfer Conference, 455 (1989).

14. Wohl, K.: Trans. American Inst. Chemical Engineers 42, 215 (1946).

15. Groff, E. G. and Faeth, G. M.: Characteristics of a Steadily Operating Metal Combustor, Technical Report to Defense Advanced Research Projects Agency, Contract N00600-74-0033, Program Code 2N10, ARPA order No. 2150 (1976).

16. Groff, E. G. and Faeth, G. M.: Ind. Eng. Chem. Fundam. 17, 326 (1978).

17. Lewis, G. N. and Randall, M.: Thermodynamics, 2nd ed. Revised by Pitzer K. S. and Brewer, L., McGraw-Hill, N.Y. 57 (1961).

18. Gordon, S. and McBride, B. J.: Computer Program for Calculation of Complex Chemical Equilibrium Composition, Rocket Performance, Incident and Reflected Shocks and Chapman-Jouget Detonation, NASA SP-273, Washington, D.C. (1971).

19. Dworkin, A. S., Bronstein, H. R., and Bredig, M. A.: J. Phys. Chem. 66, 572 (1962).

20. Weimer, J. C., Faeth, G. M., and Olsen, D. R.: AIChE J. 19, 552 (1973).

Table 1. Subcooling effects on plume length

T_∞ K	Subcooling ΔT, K	ρ_∞ Kg/m^3	ρ_o Kg/m^3	C_p $\frac{KJ}{Kg\ of\ Li}$	ΔH_r $\frac{KJ}{Kg\ of\ SF_6}$	$\frac{L}{d}$
1130	479	449	5.97	4.13	19,267	5.66
1358	251	426	5.97	4.11	19,116	11.64
1415	194	421	5.97	4.10	19,079	36.44
1586	23	403	5.97	4.10	18,966	132.42

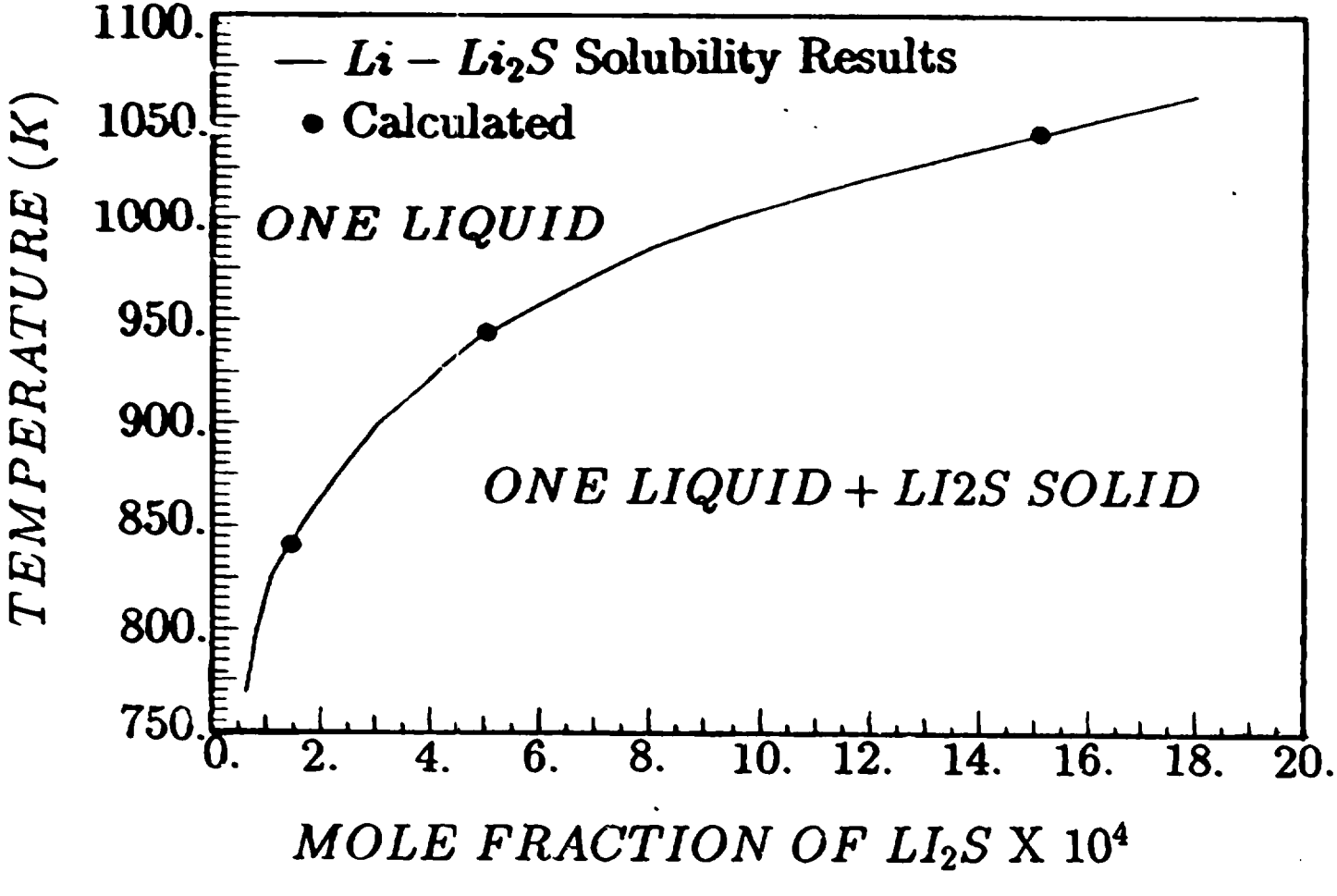

Fig.1 Solubility Comparison Between Prediction(dots) and Data of $Li - Li_2S$ System

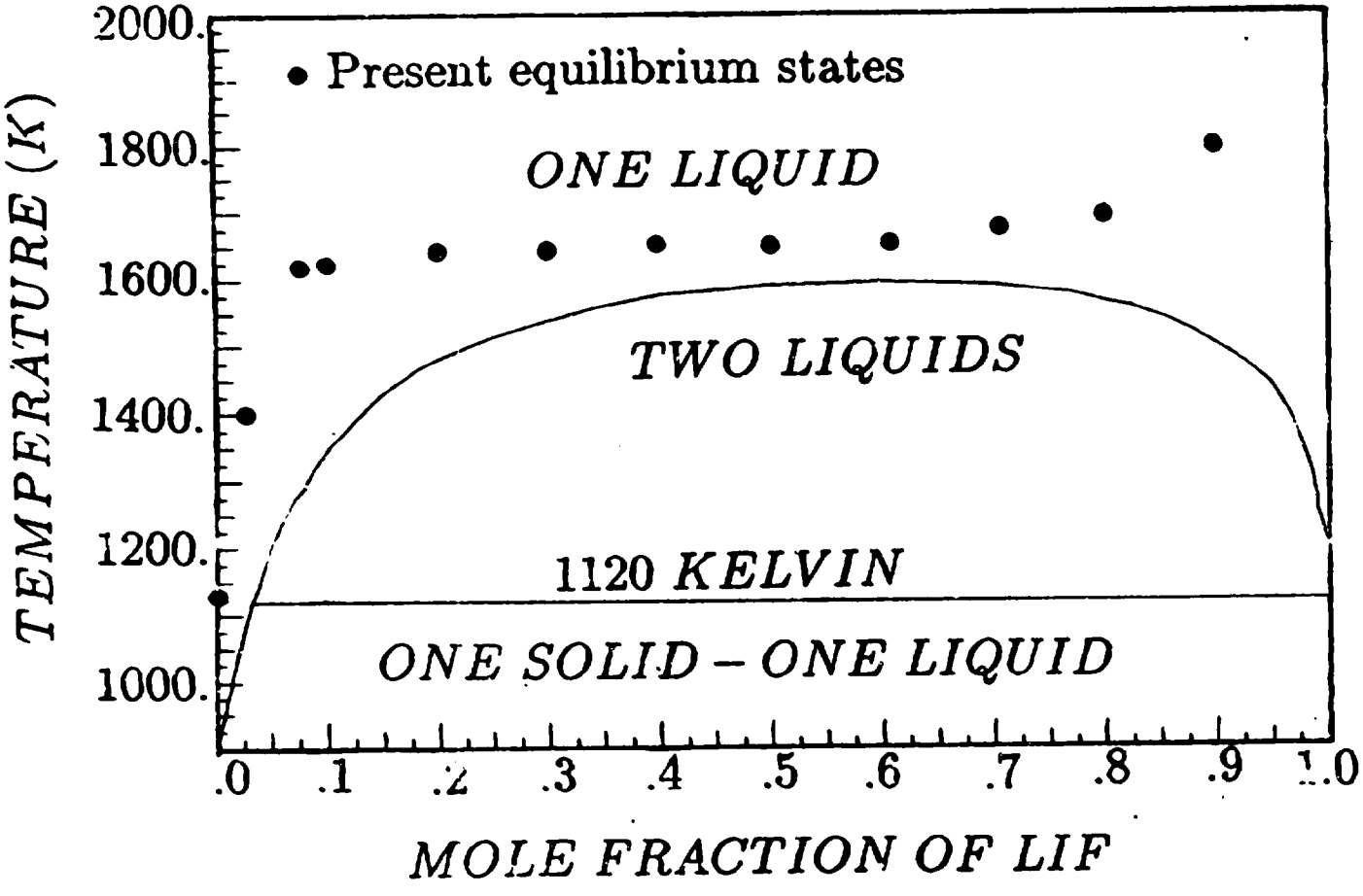

Fig.2 Equilibrium States (of Molten Li fuel at T_∞=1130 K reacting with gaseous SF_6 at T_0=298 K) Phase Diagram

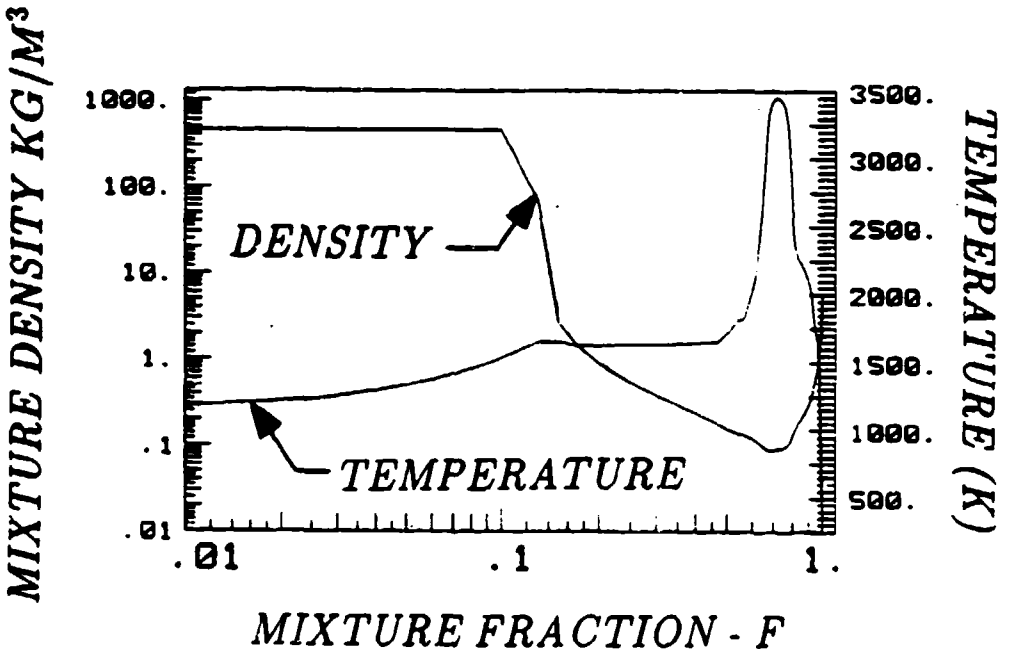

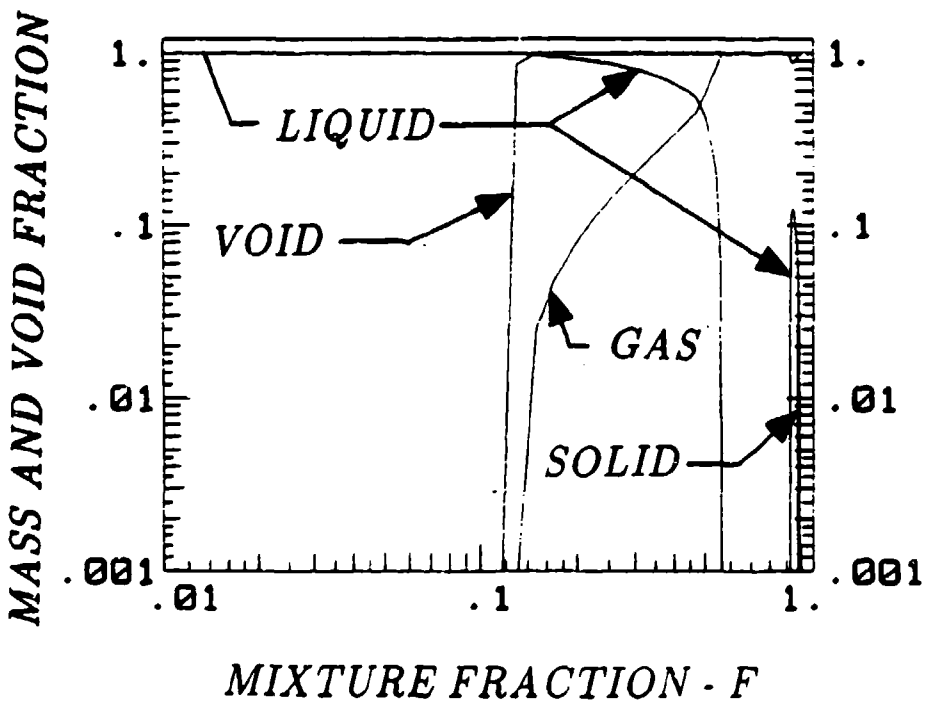

Fig.3 Equations of States For $Li - SF_6$ System with Li at 1130 K and SF_6 Gas at 298 K

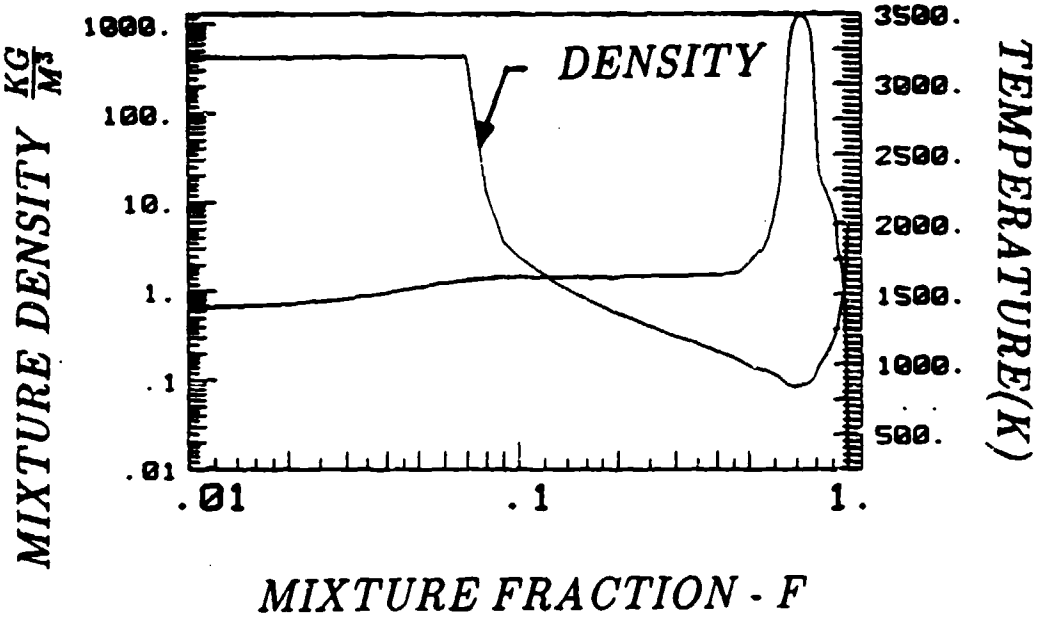

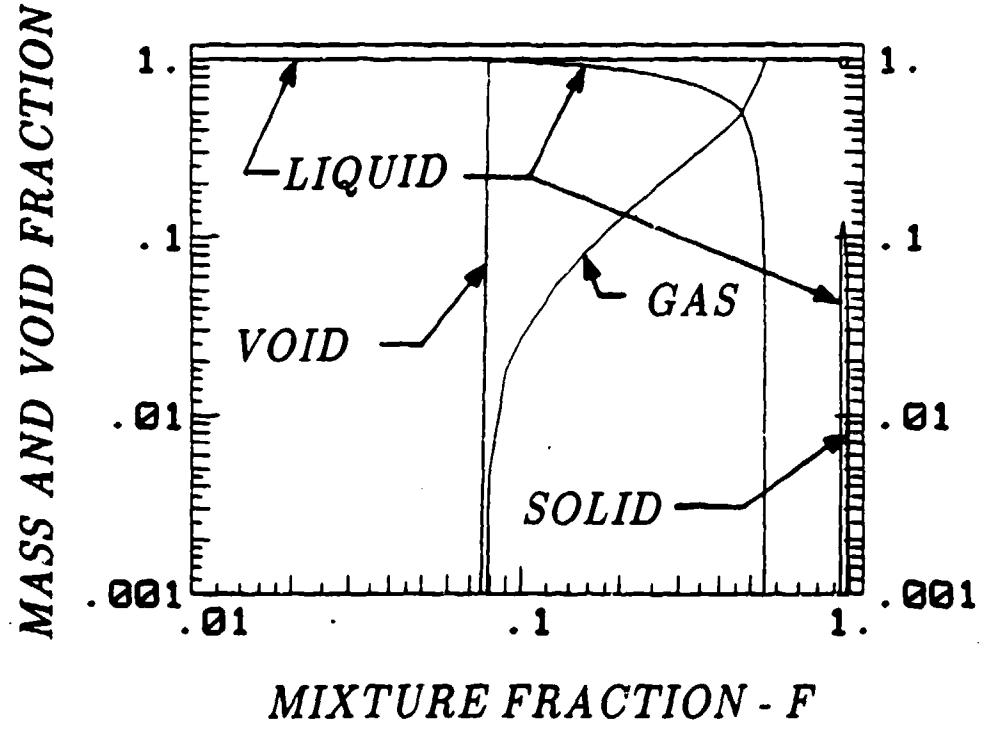

Fig.4 Equations of States For $Li - SF_6$ System with Li at 1358 K and SF_6 Gas at 298 K

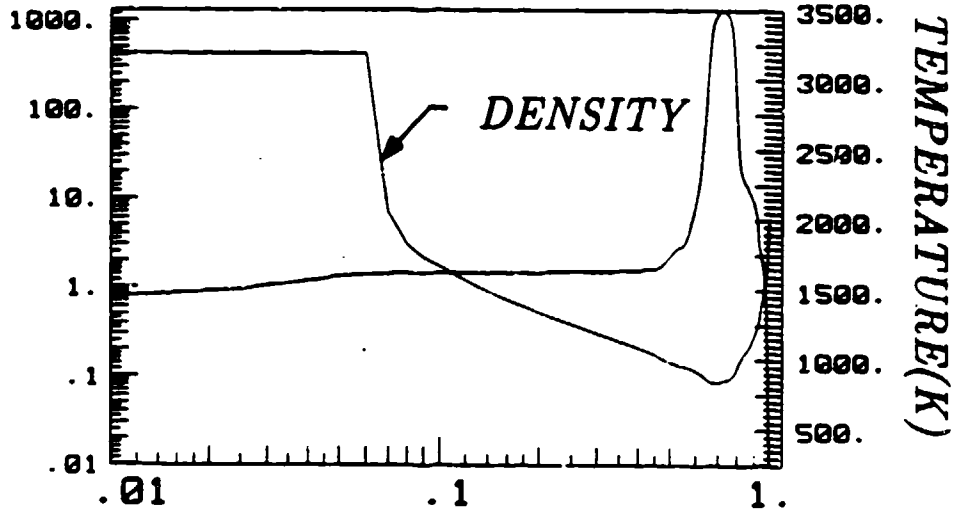

MIXTURE FRACTION - F

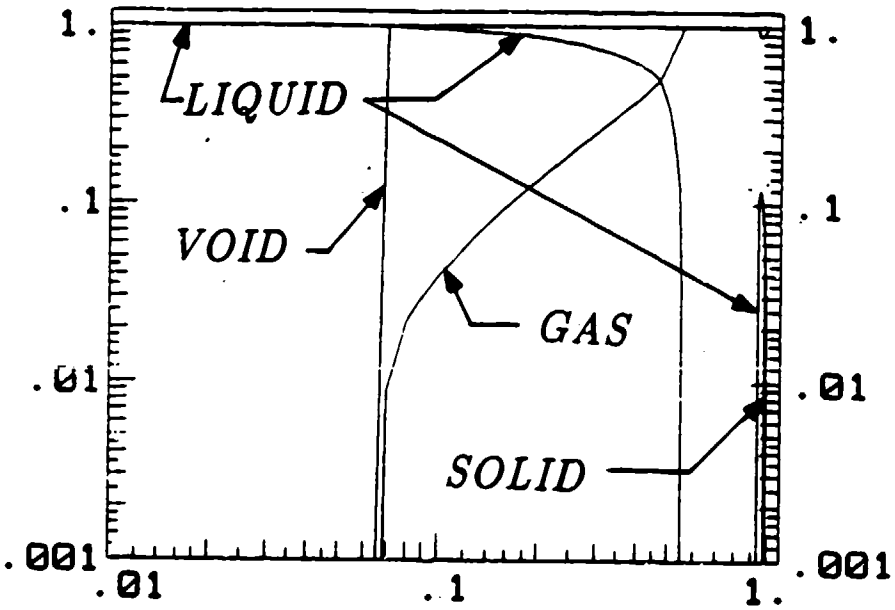

MIXTURE FRACTION- F

Fig.5 Equations of States For $Li - SF_6$ System with Li at 1415 K and SF_6 Gas at 298 K

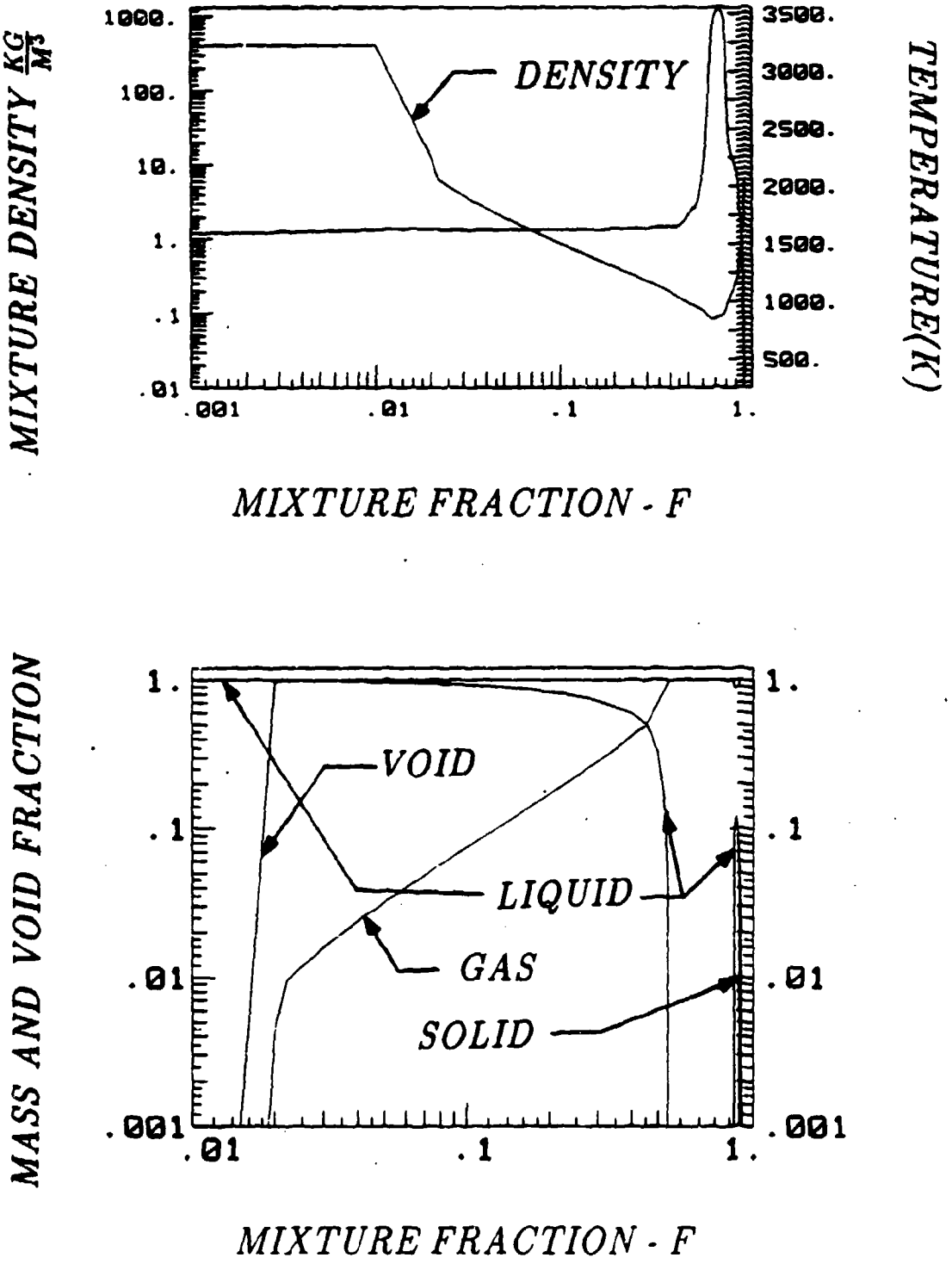

Fig.6 Equations of States For $Li - SF_6$ System with Li at 1586 K and SF_6 Gas at 298 K

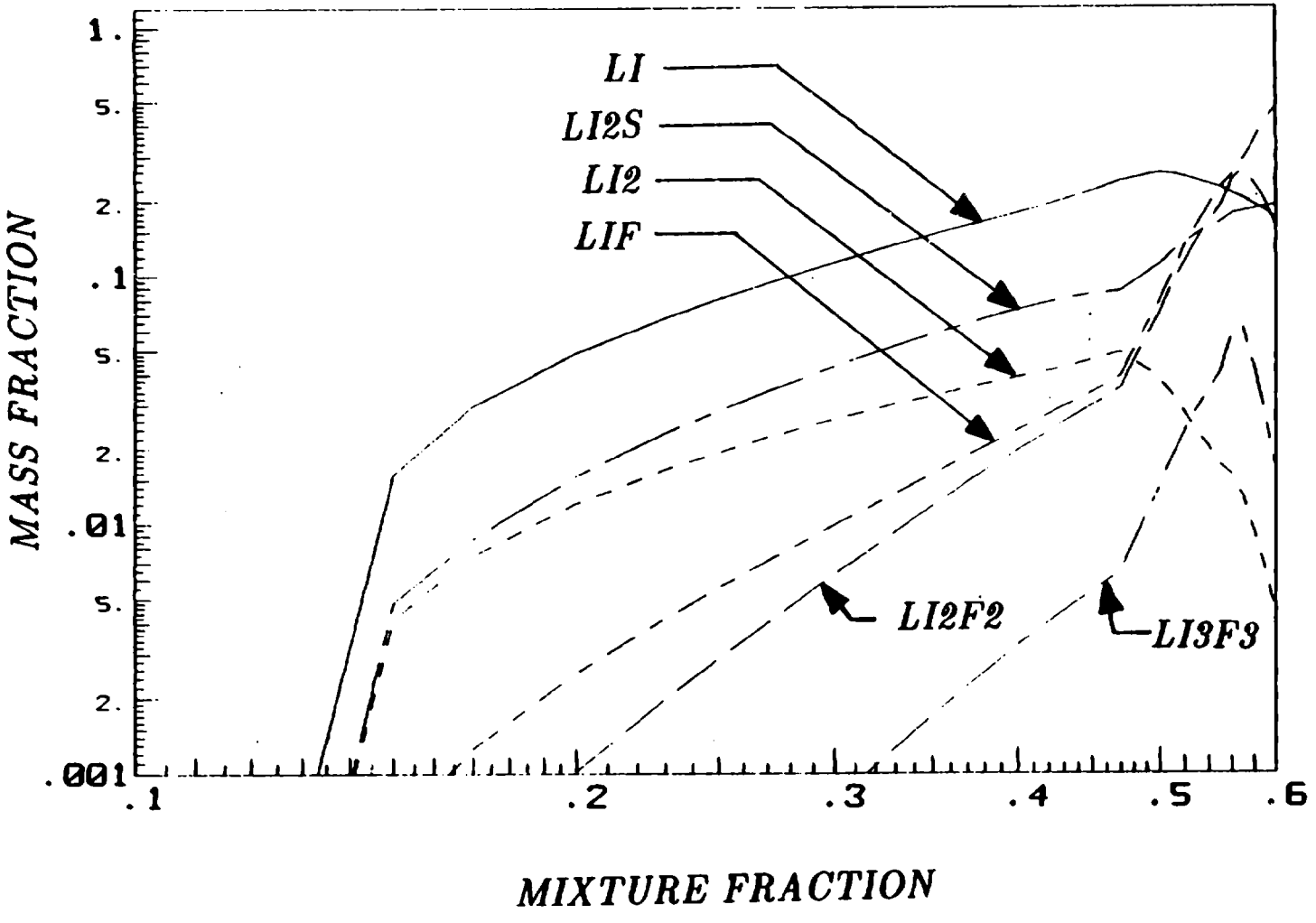

Fig.7 Equilibrium Compositions of $Li - SF_6$ System with Li at 1130 K and SF_6 Gas at 298 K

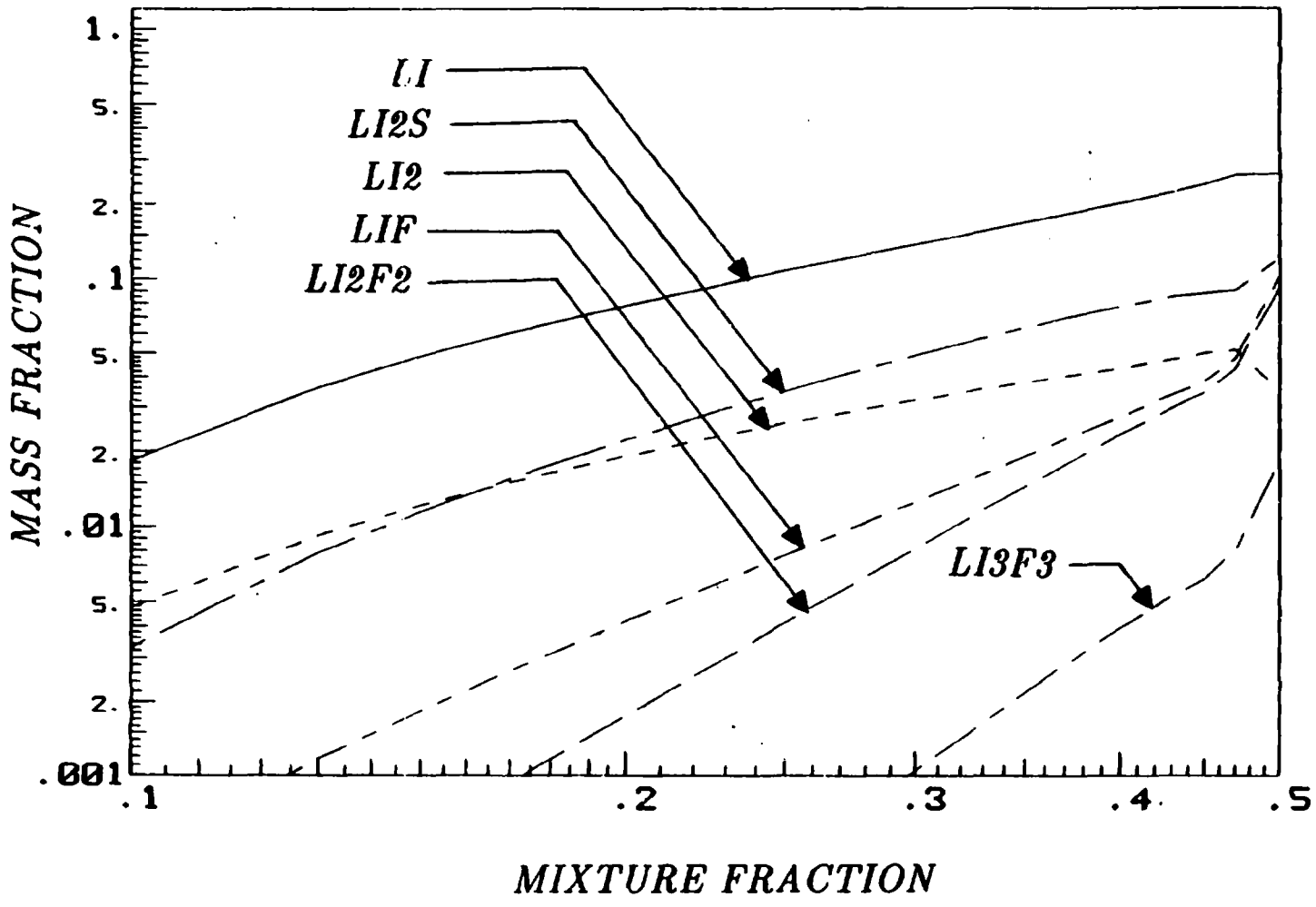

Fig.8 Equilibrium Compositions of $Li - SF_6$ System with Li at 1358 K and SF_6 Gas at 298 K

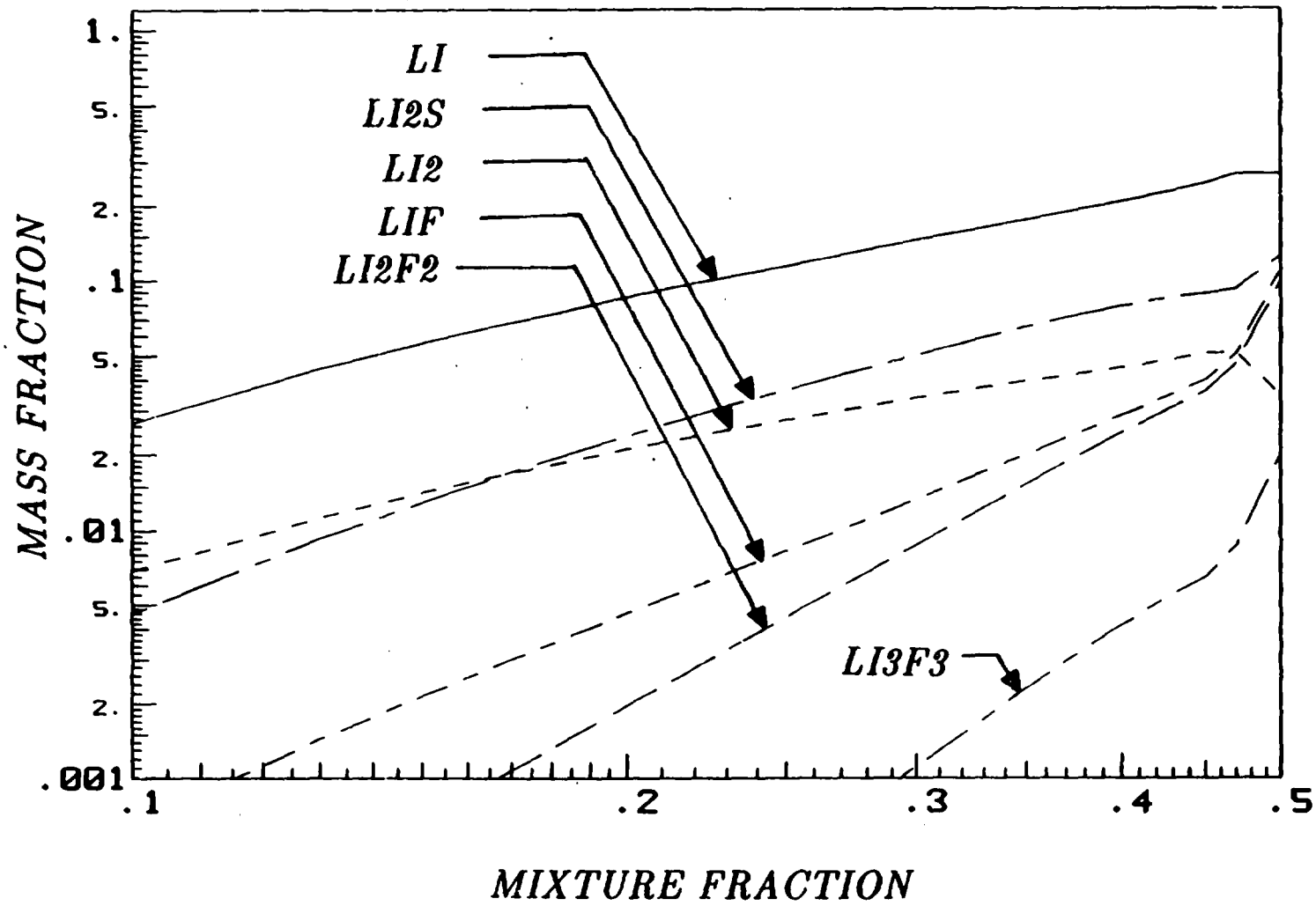

Fig.9 Equilibrium Compositions of $Li - SF_6$ System with Li at 1415 K and SF_6 Gas at 298 K

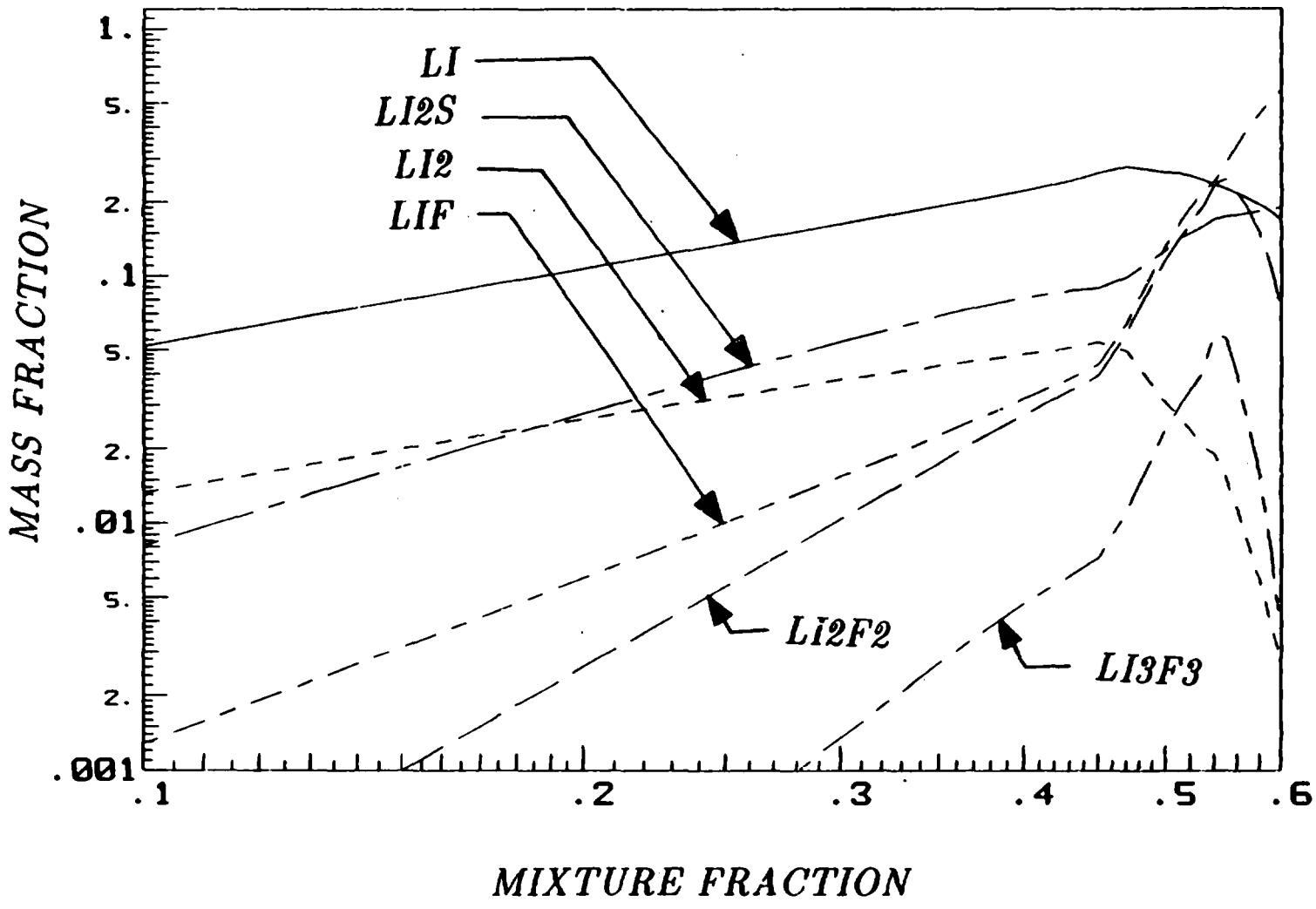

Fig.10 Equilibrium Compositions of $Li - SF_6$ System with Li at 1586 K and SF_6 Gas at 298 K

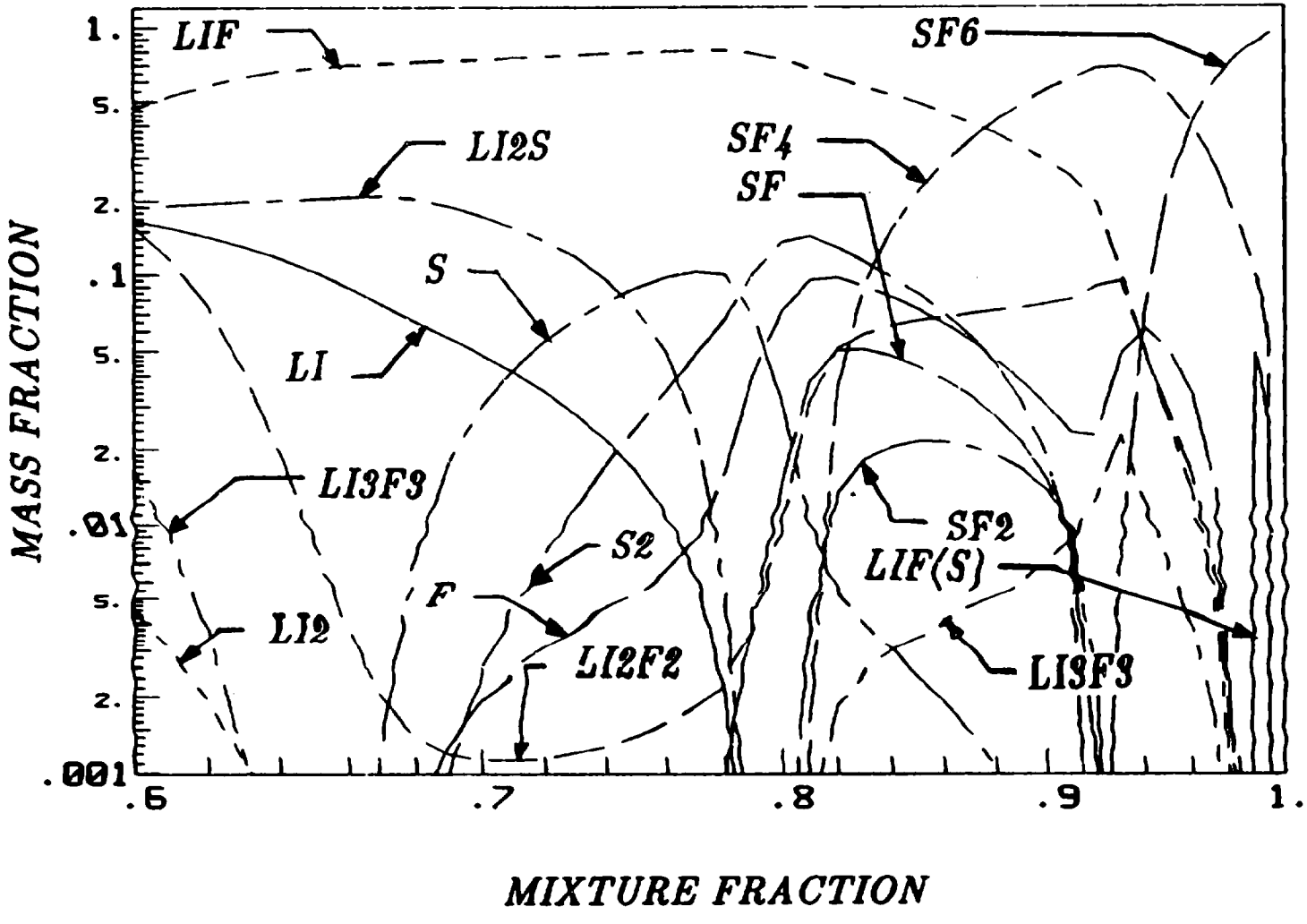

Fig.11 Equilibrium Compositions of $Li - SF_6$ System with Li at 1130 K and SF_6 Gas at 298 K

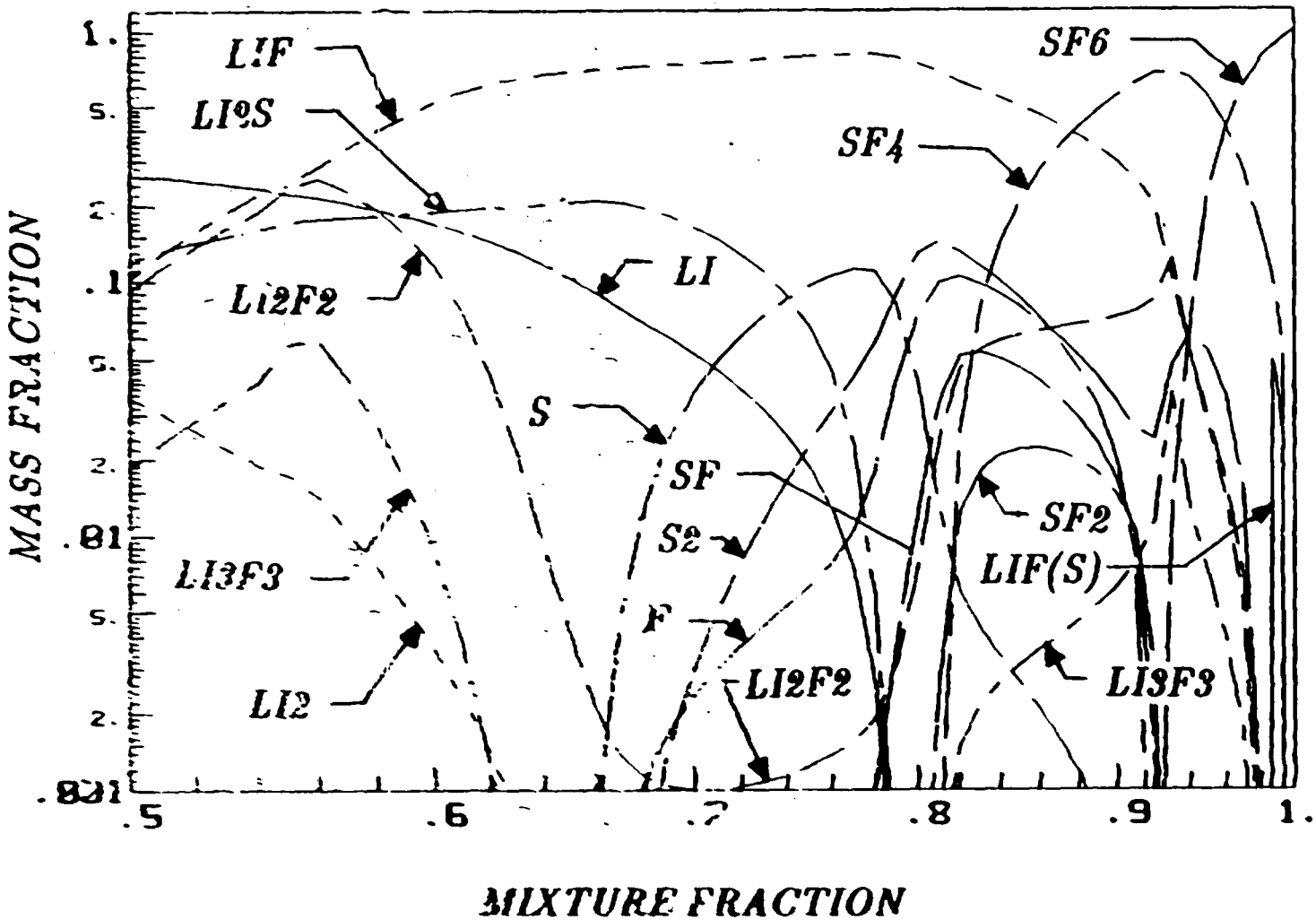

Fig. 17 Equilibrium Composition of Li – SF_6 System with Li at 1358 K and SF_6 Gas at 298 K

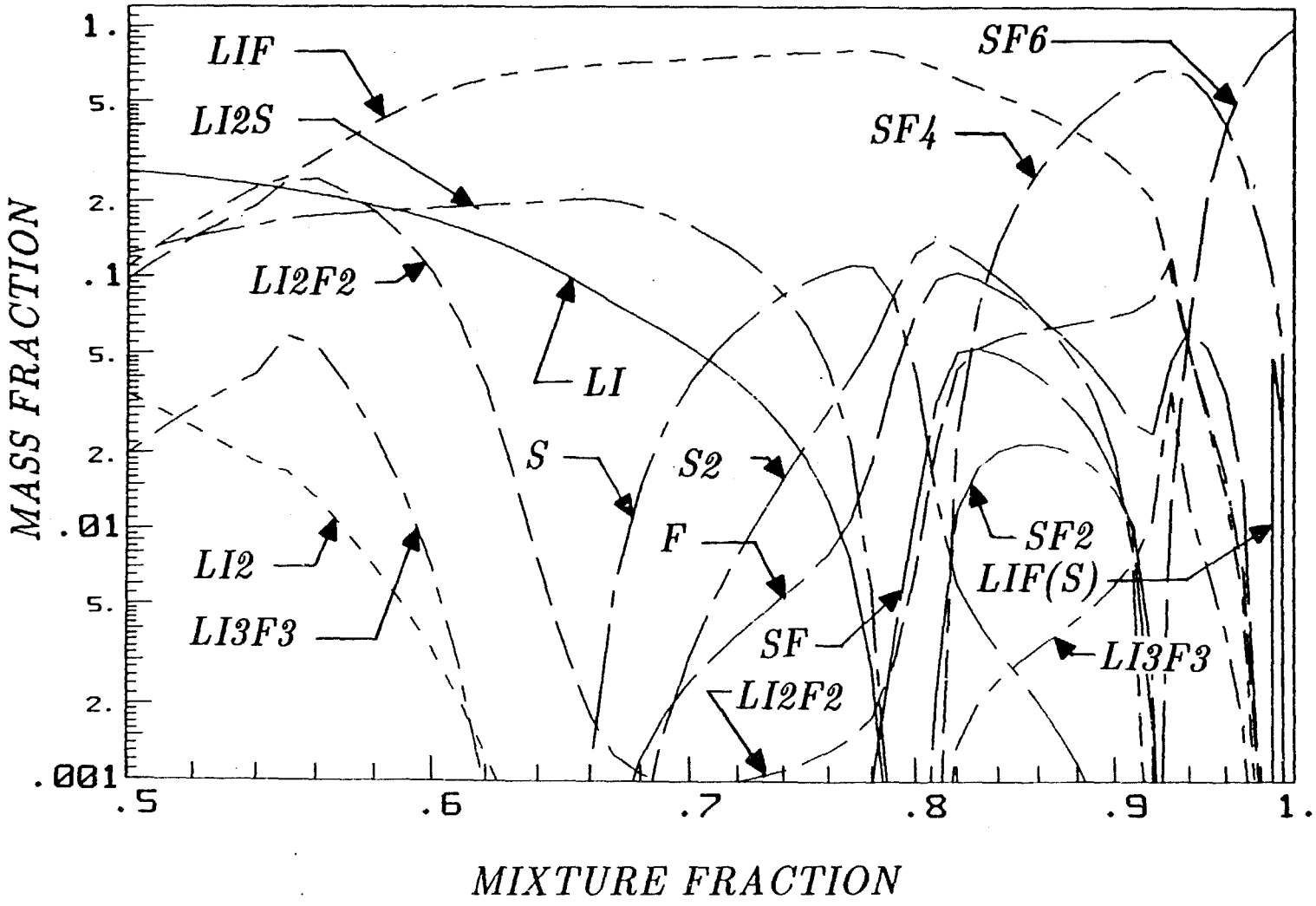

Fig.13 Equilibrium Compositions of $Li - SF_6$ System with Li at 1415 K and SF_6 Gas at 298 K

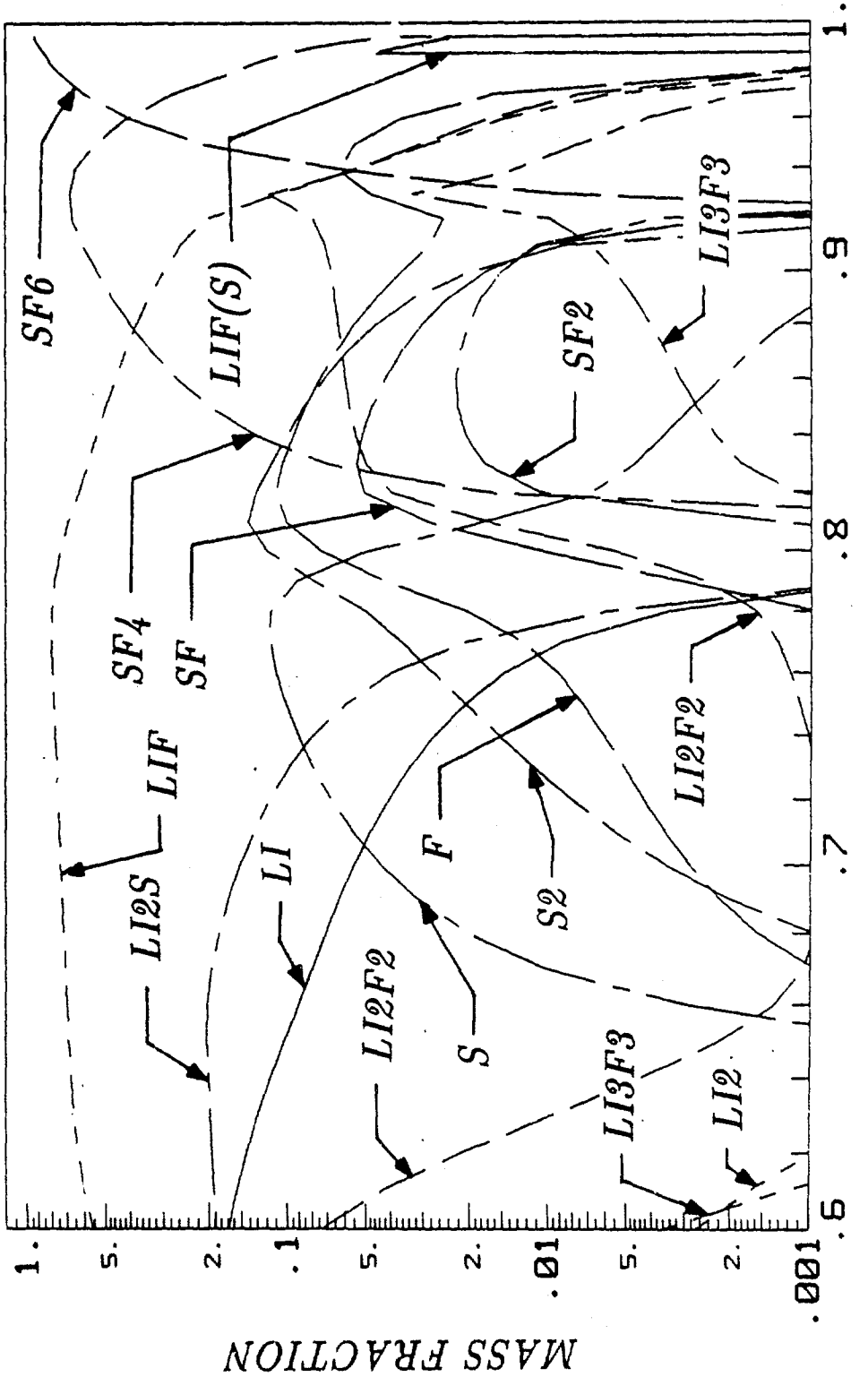

Fig.14 Equilibrium Compositions of $Li - SF_6$ System with Li at 1586 K and SF_6 Gas at 298 K

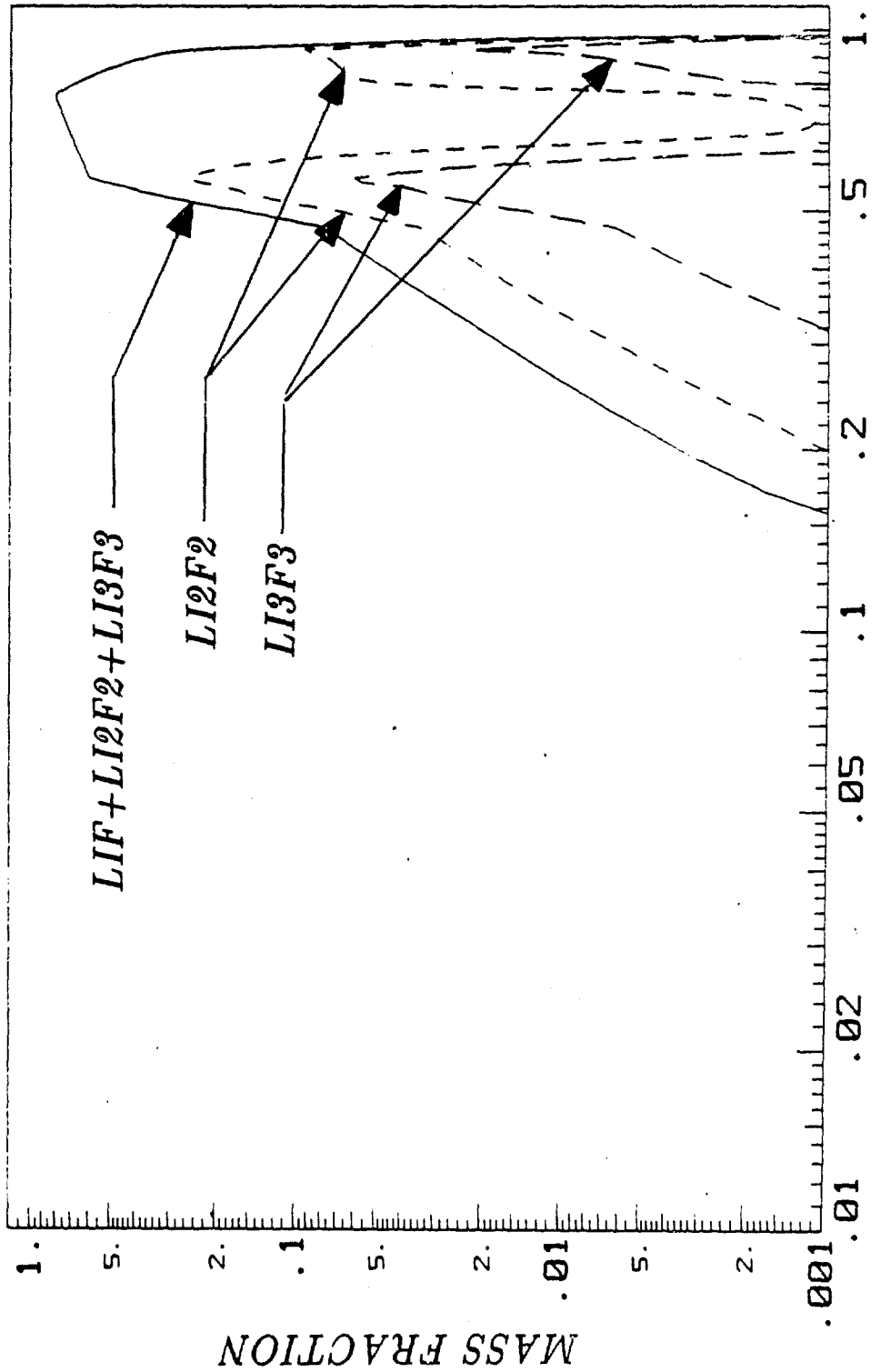

Fig.15 Equilibrium Compositions of $Li - SF_6$ System with Li at 1130 K and SF_6 Gas at 298 K

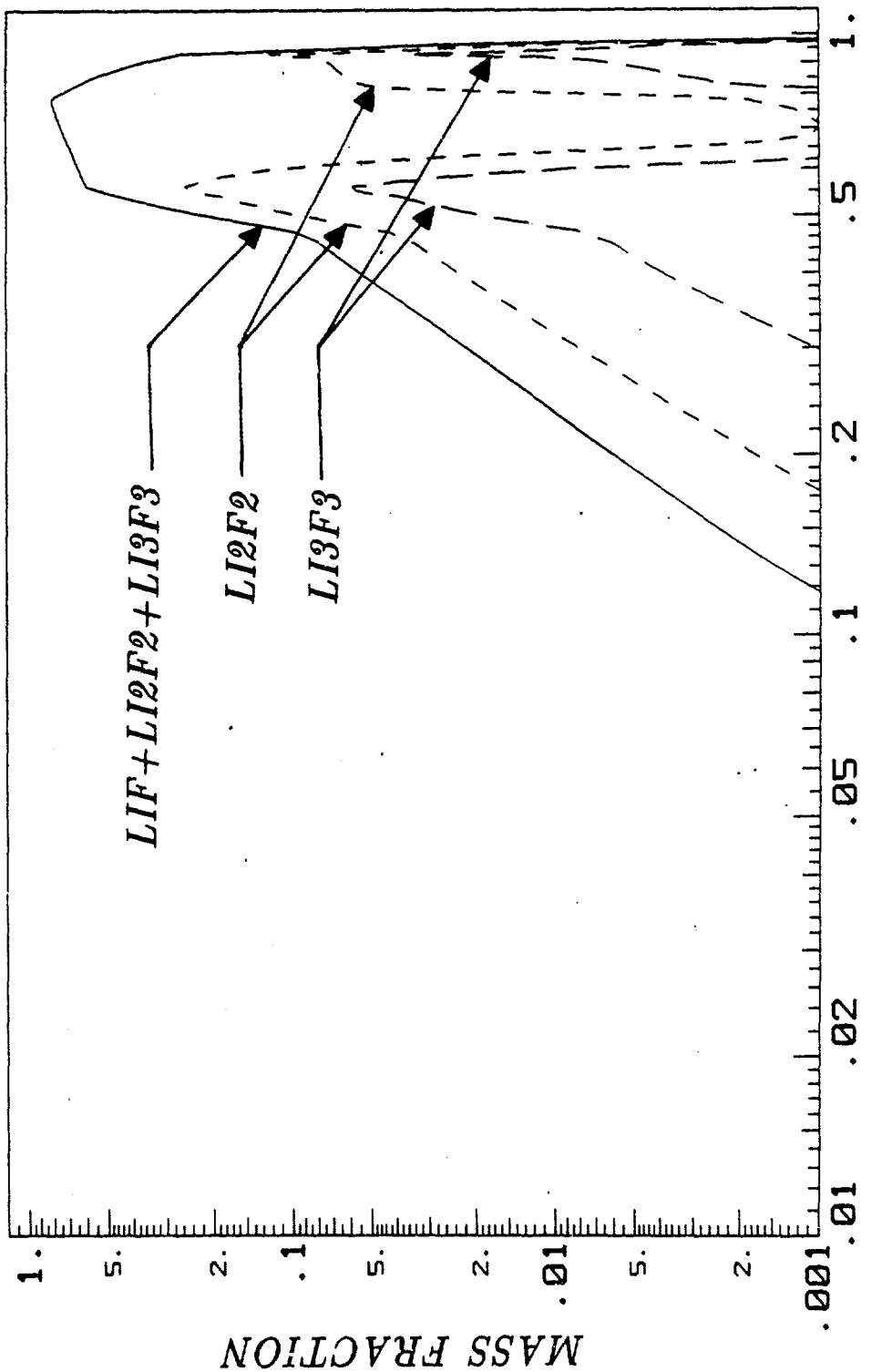

Fig.16 Equilibrium Compositions of $Li - SF_6$ System with Li at 1358 K and SF_6 Gas at 298 K

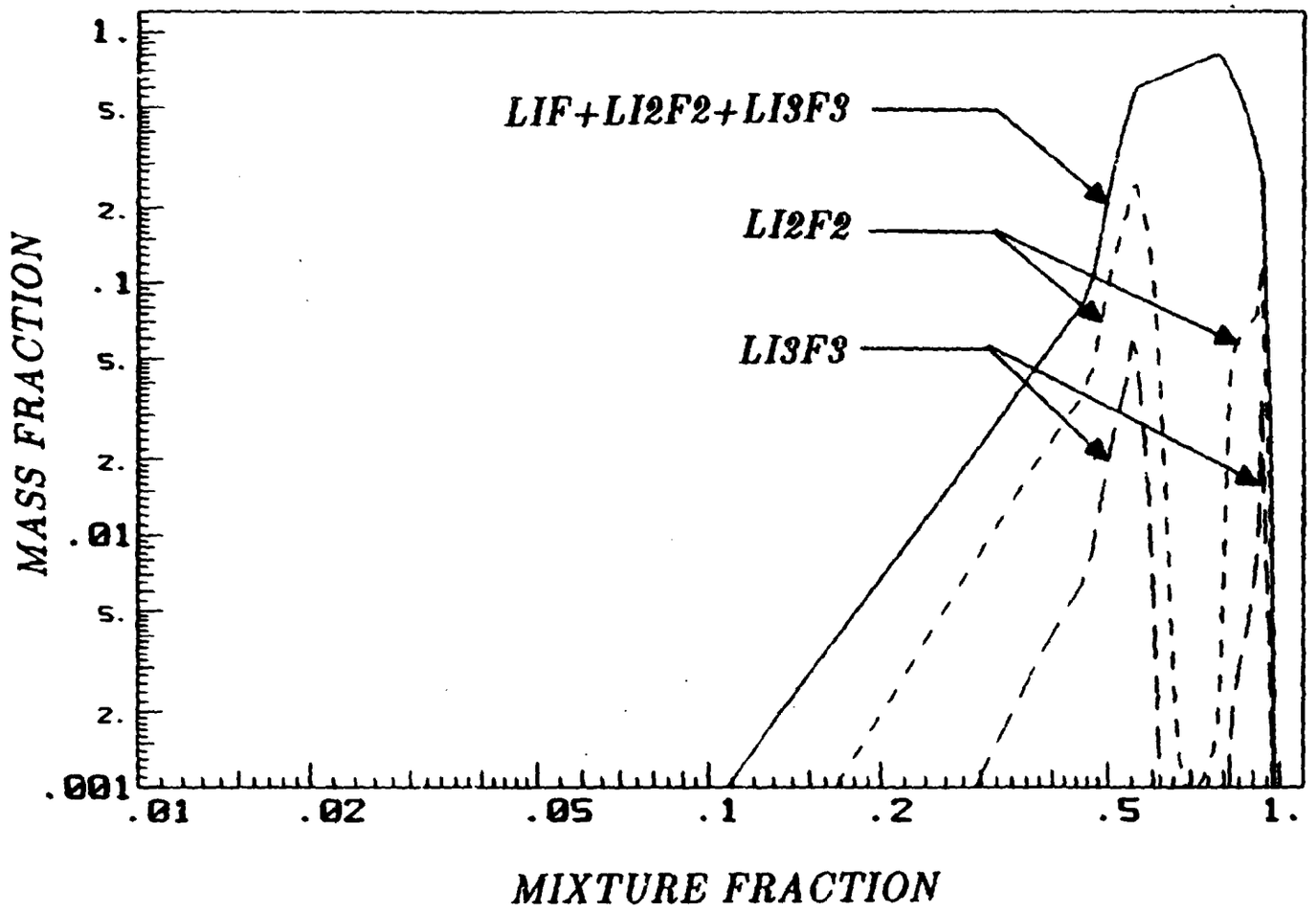

Fig.17 Equilibrium Compositions of $Li - SF_6$ System with Li at 1415 K and SF_6 Gas at 298 K

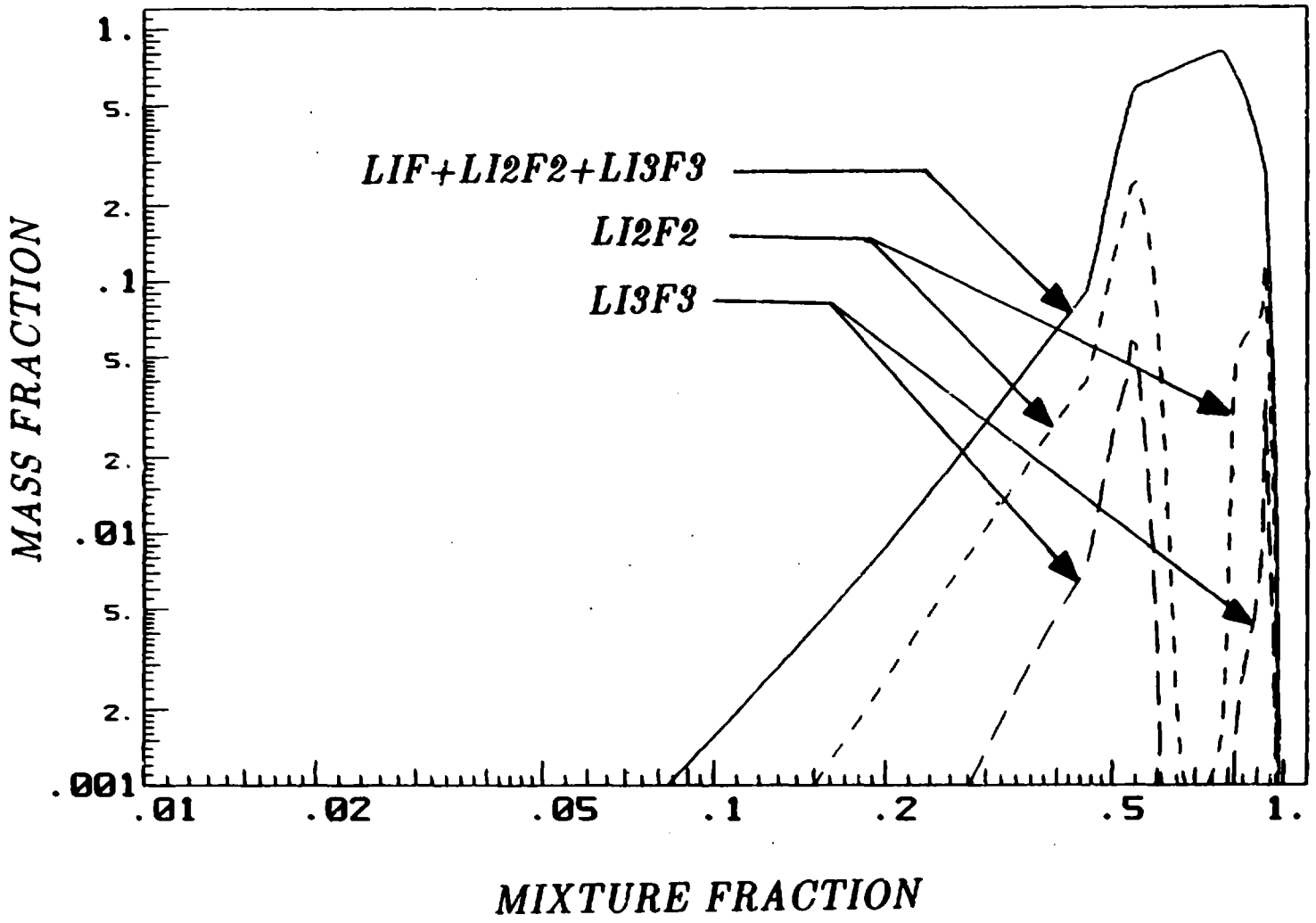

Fig.18 Equilibrium Compositions of $Li - SF_6$ System with Li at 1586 K and SF_6 Gas at 298 K

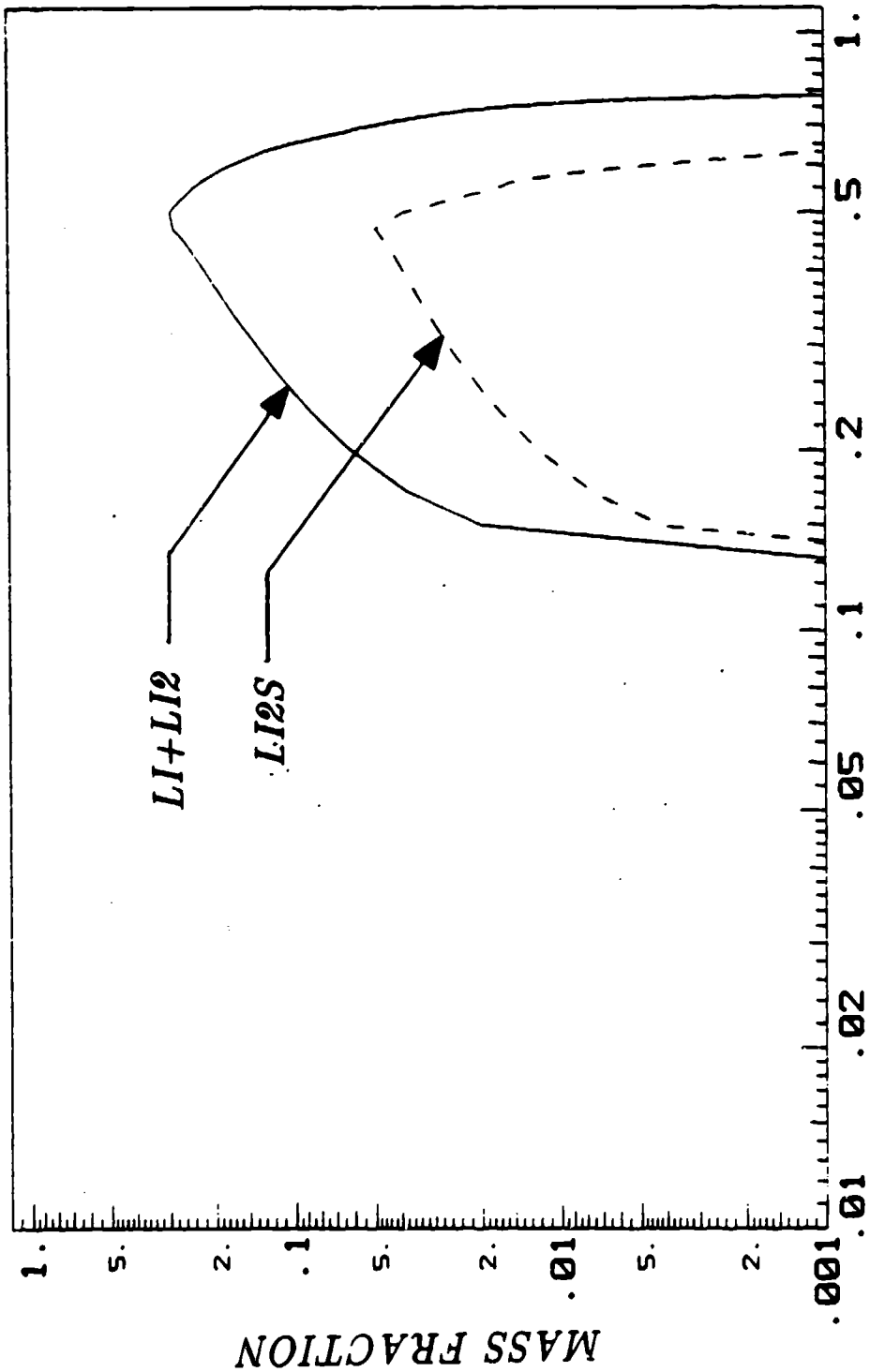

Fig.19 Equilibrium Compositions of $Li - SF_6$ System with Li at 1130 K and SF_6 Gas at 298 K

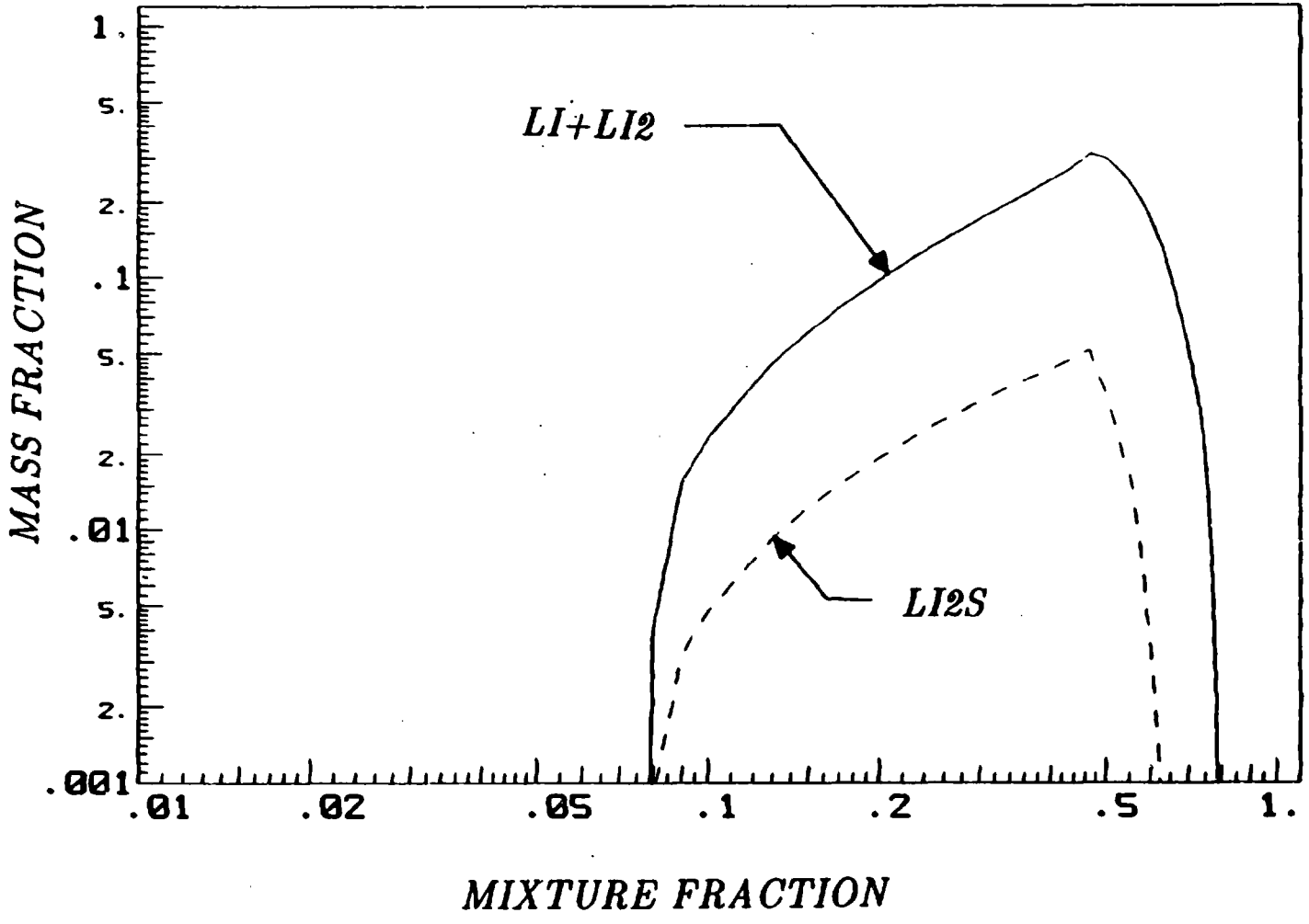

Fig.20 Equilibrium Compositions of Li - SF_6 System with Li at 1358 K and SF_6 Gas at 298 K

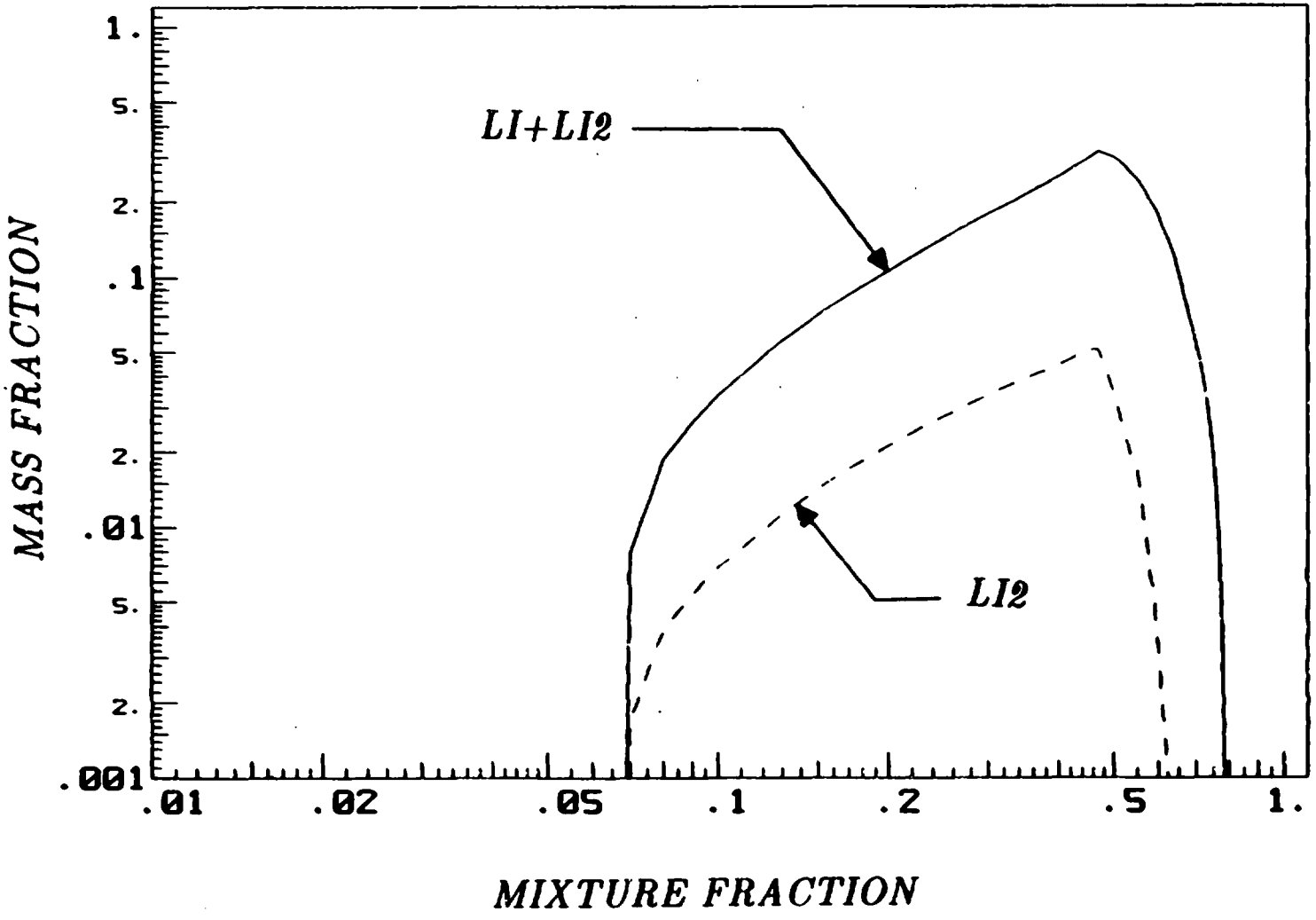

Fig.21 Equilibrium Compositions of $Li - SF_6$ System with Li at 1415 K and SF_6 Gas at 298 K

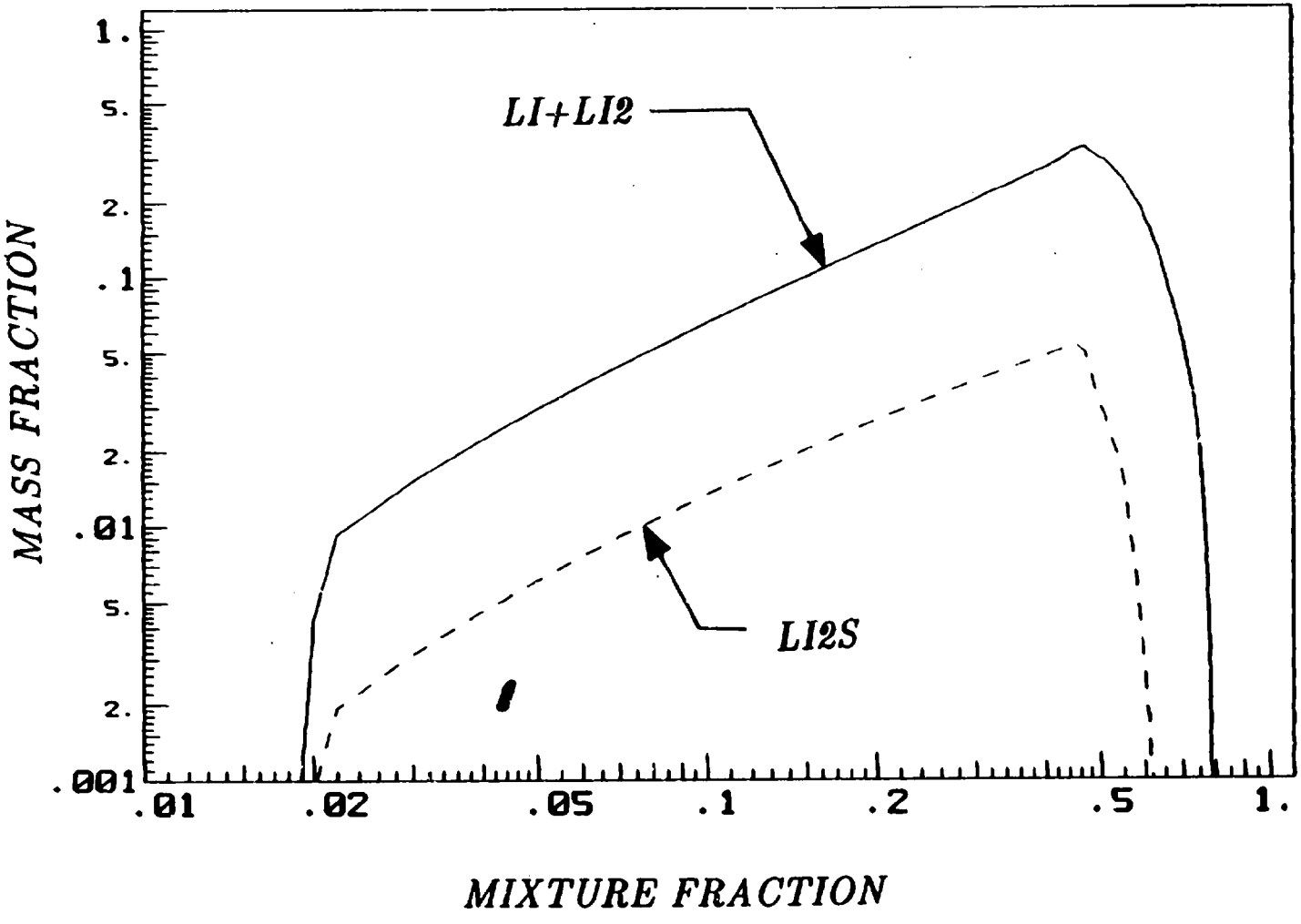

Fig.22 Equilibrium Compositions of $Li - SF_6$ System with Li at 1586 K and SF_6 Gas at 298 K

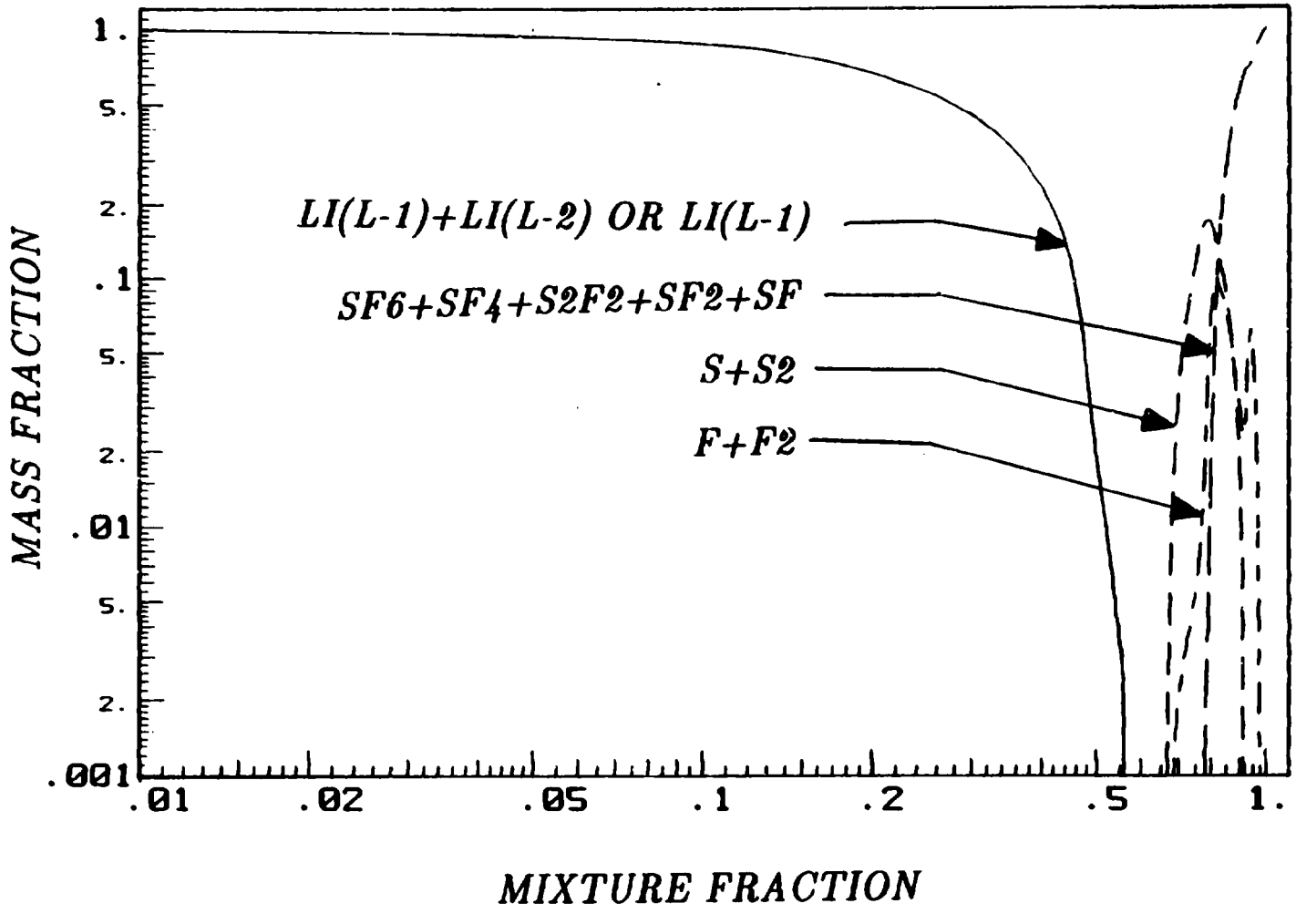

Fig.23 Equilibrium Compositions of $Li - SF_6$ System with Li at 1130 K and SF_6 Gas at 298 K

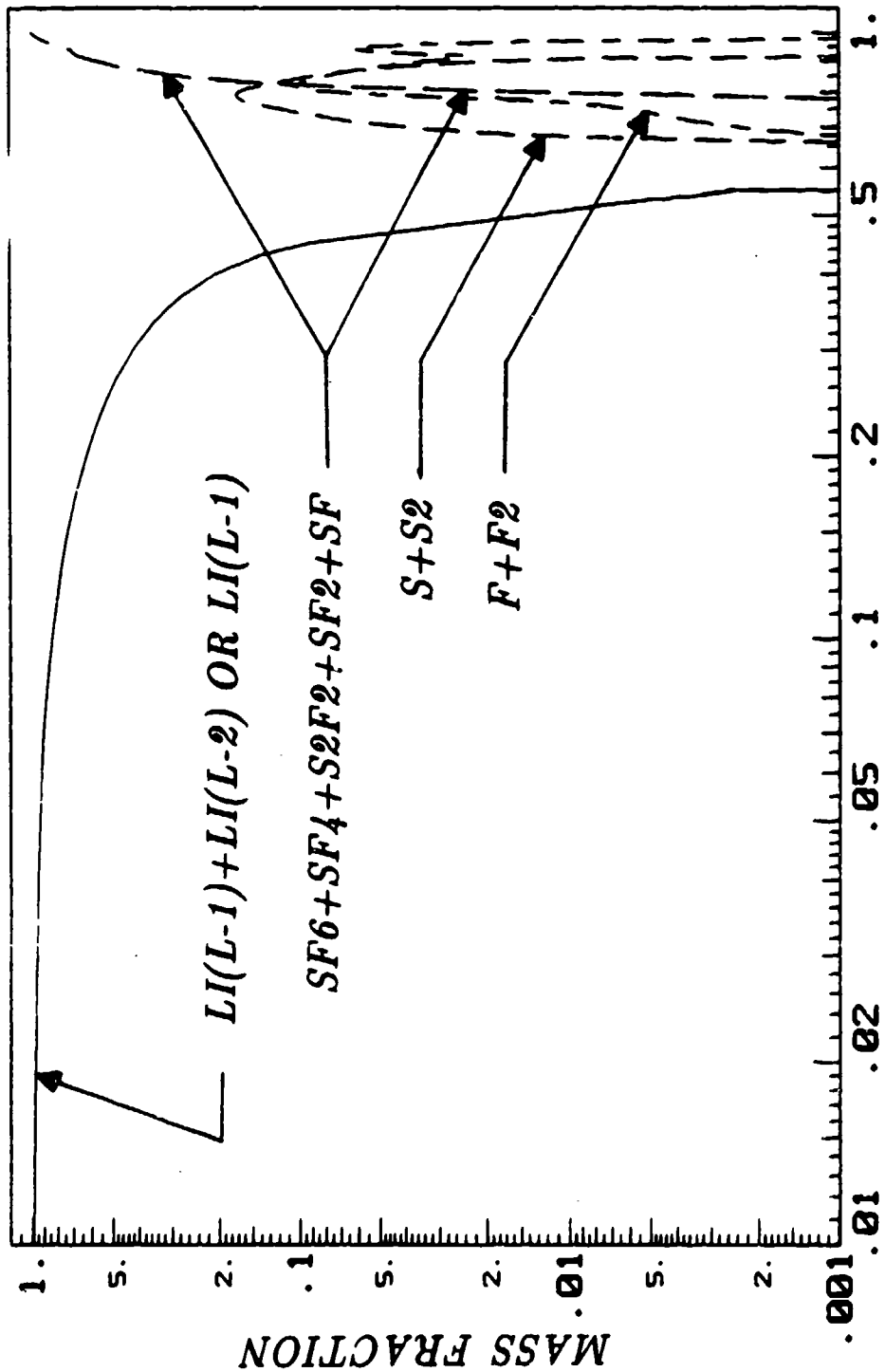

Fig.24 Equilibrium Compositions of $Li - SF_6$ System with Li at 1358 K and SF_6 Gas at 298 K

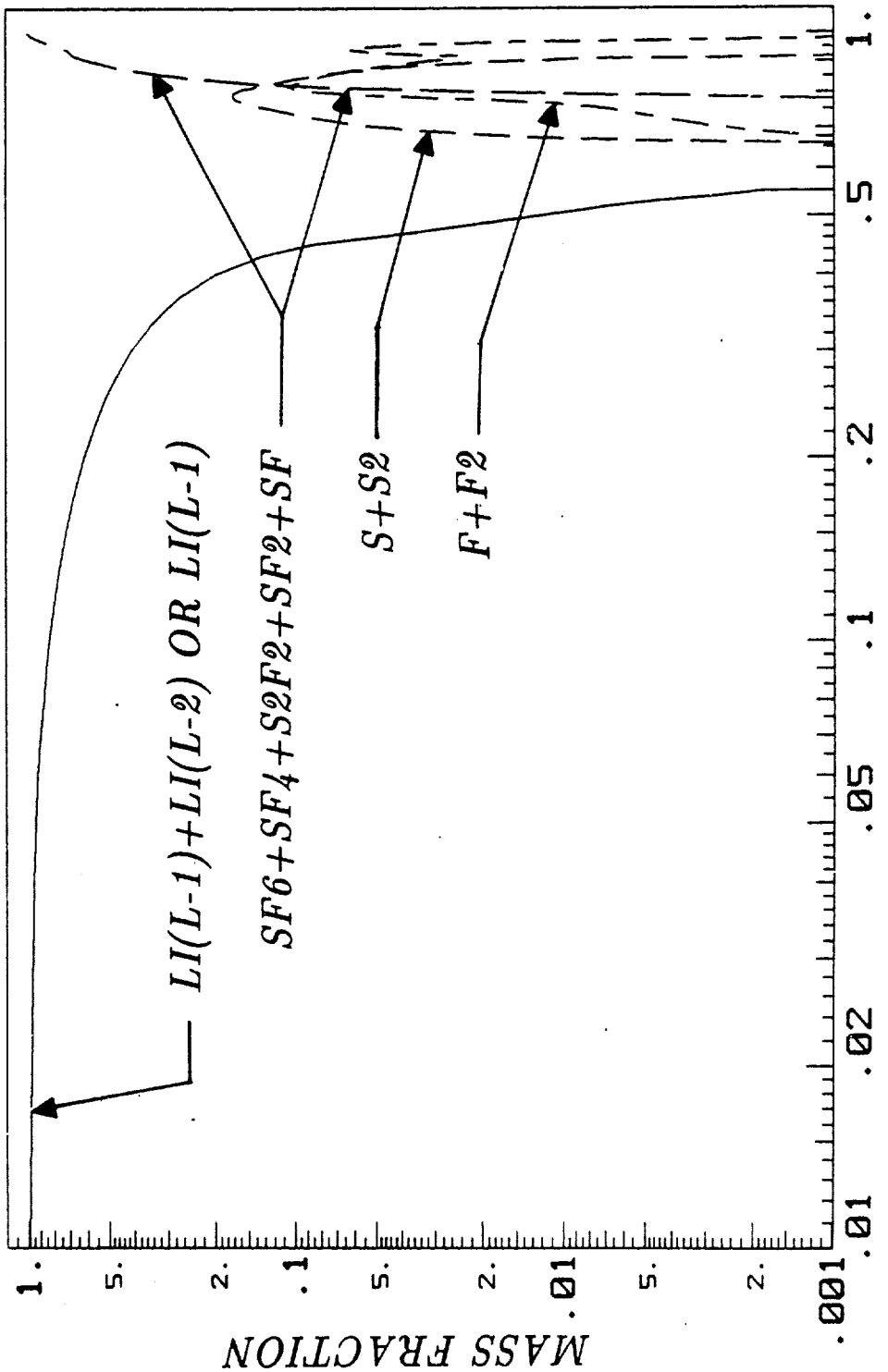

Fig.25 Equilibrium Compositions of $Li - SF_6$ System with Li at 1415 K and SF_6 Gas at 298 K

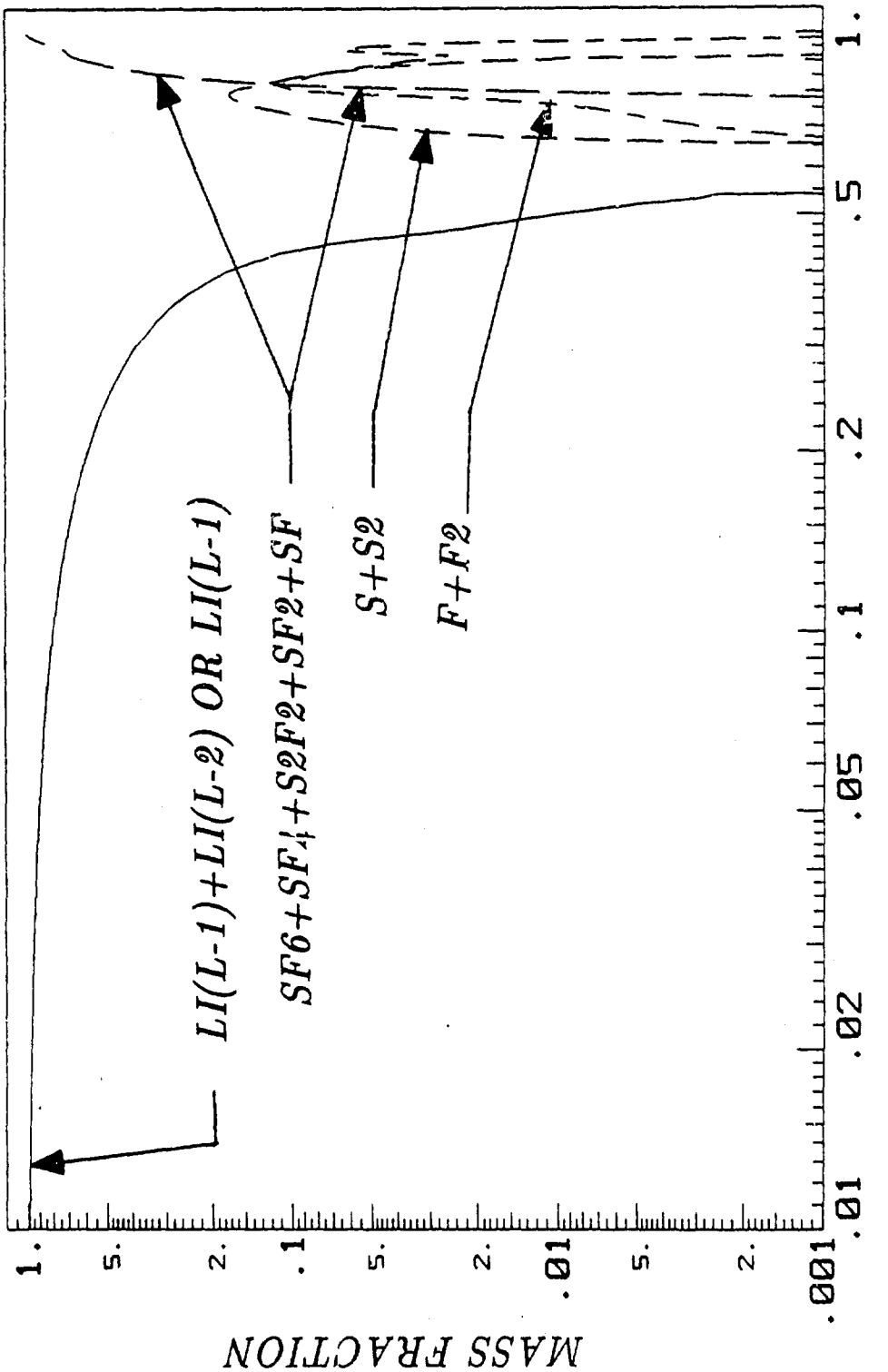

Fig.26 Equilibrium Compositions of $Li - SF_6$ System with Li at 1586 K and SF_6 Gas at 298 K

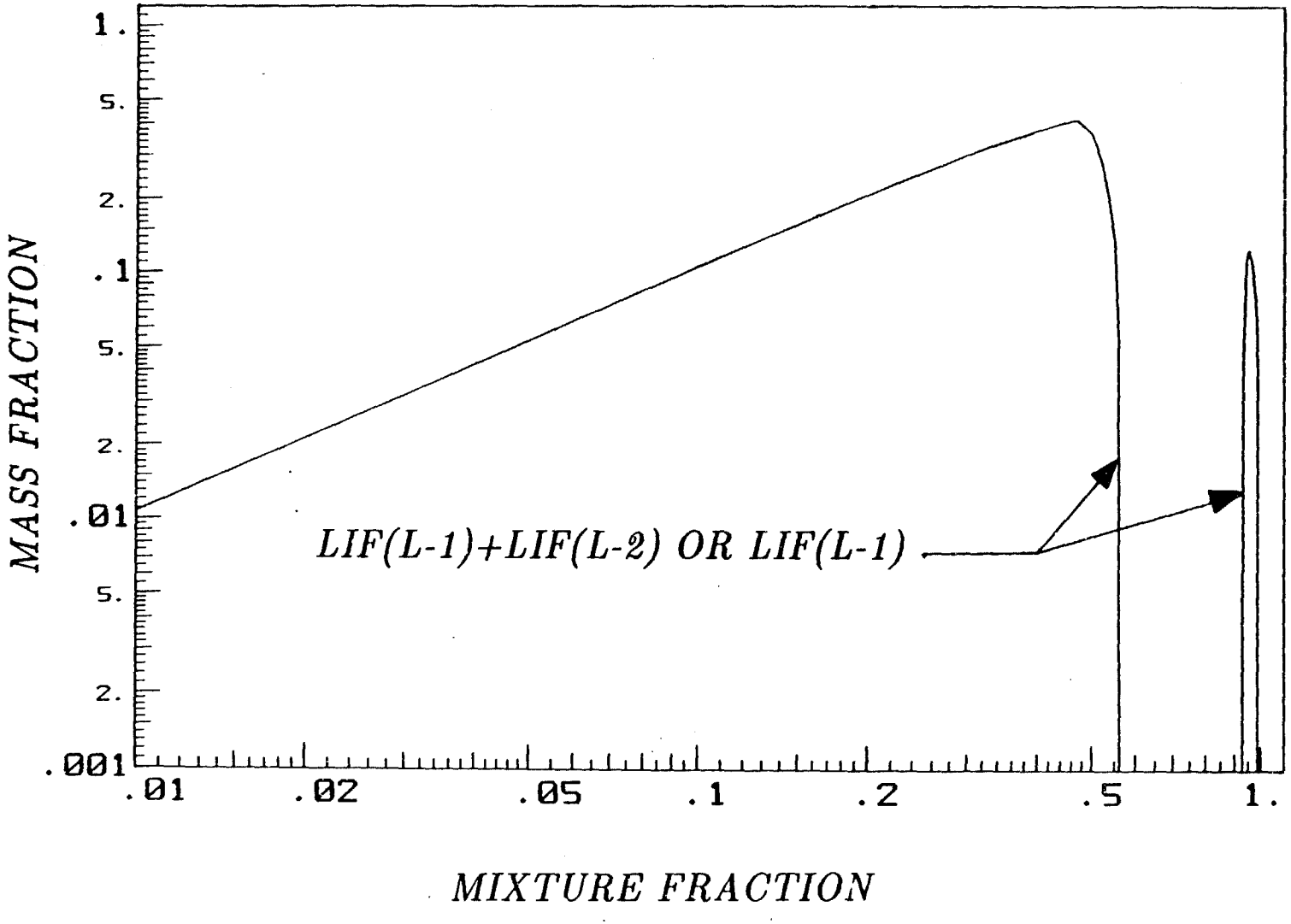

Fig.27 Equilibrium Compositions of $Li - SF_6$ System with Li at 1130 K and SF_6 Gas at 298 K

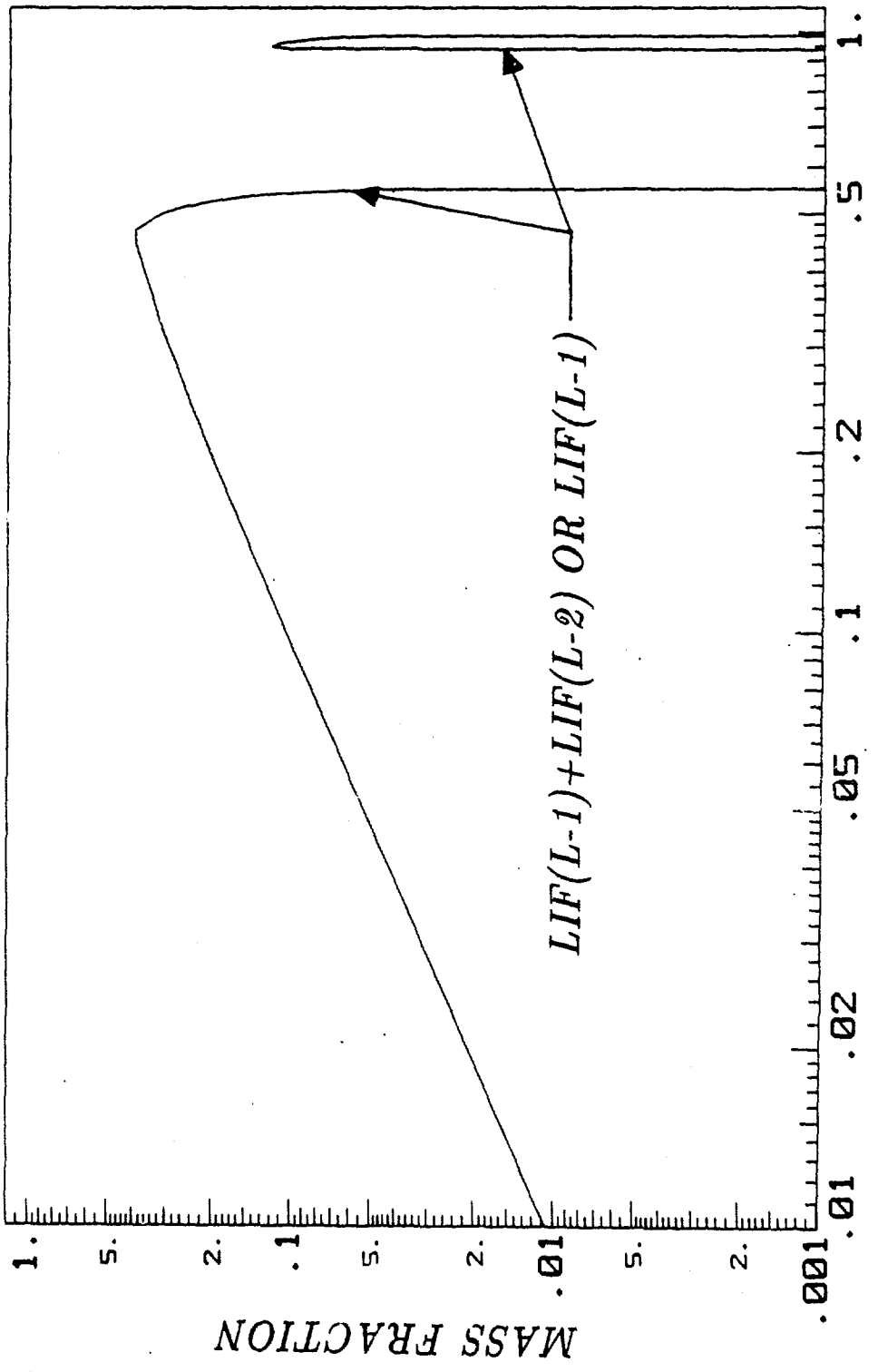

Fig.28 Equilibrium Compositions of $Li - SF_6$ System with Li at 1358 K and SF_6 Gas at 298 K

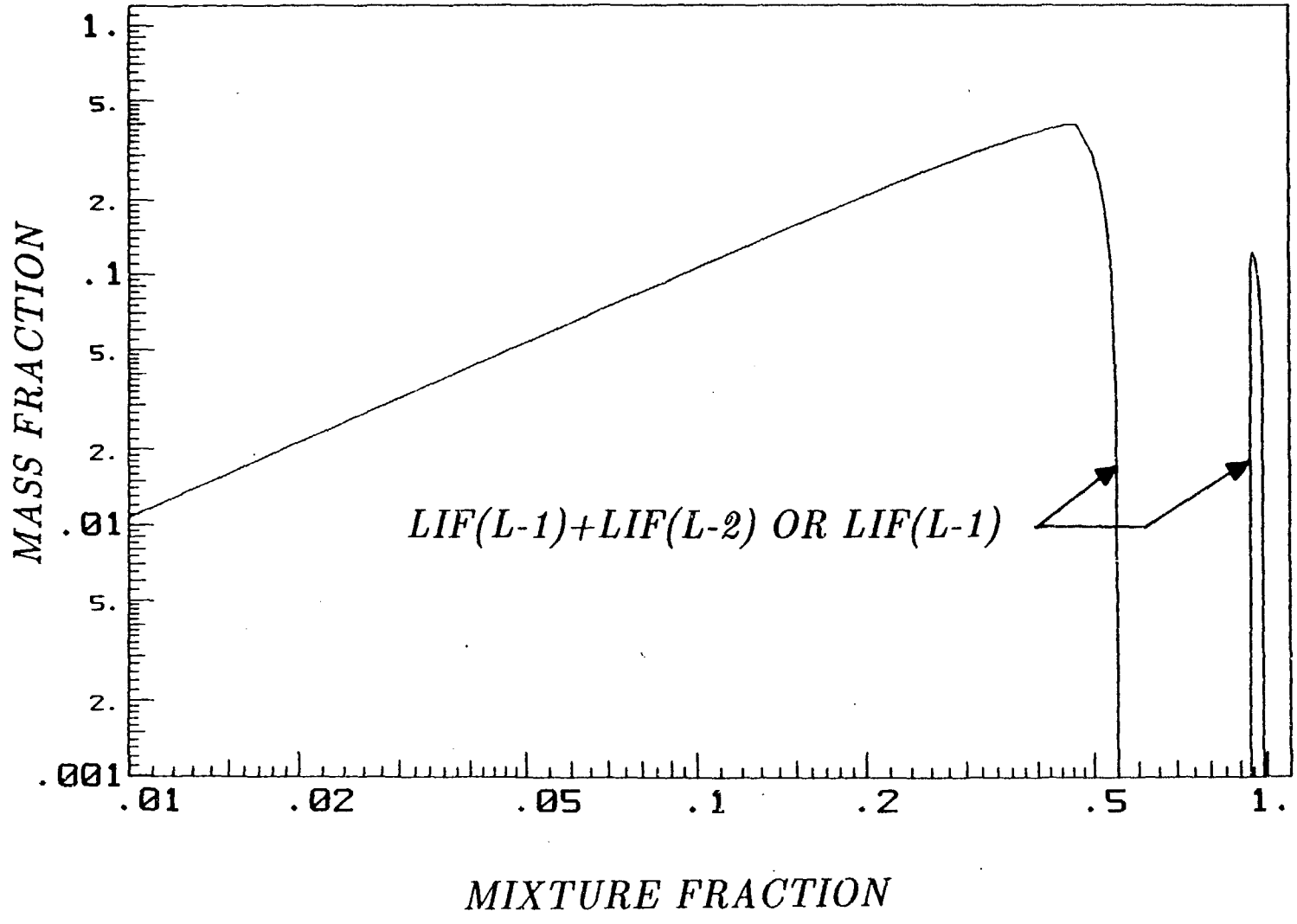

Fig.29 Equilibrium Compositions of $Li - SF_6$ System with Li at 1415 K and SF_6 Gas at 298 K

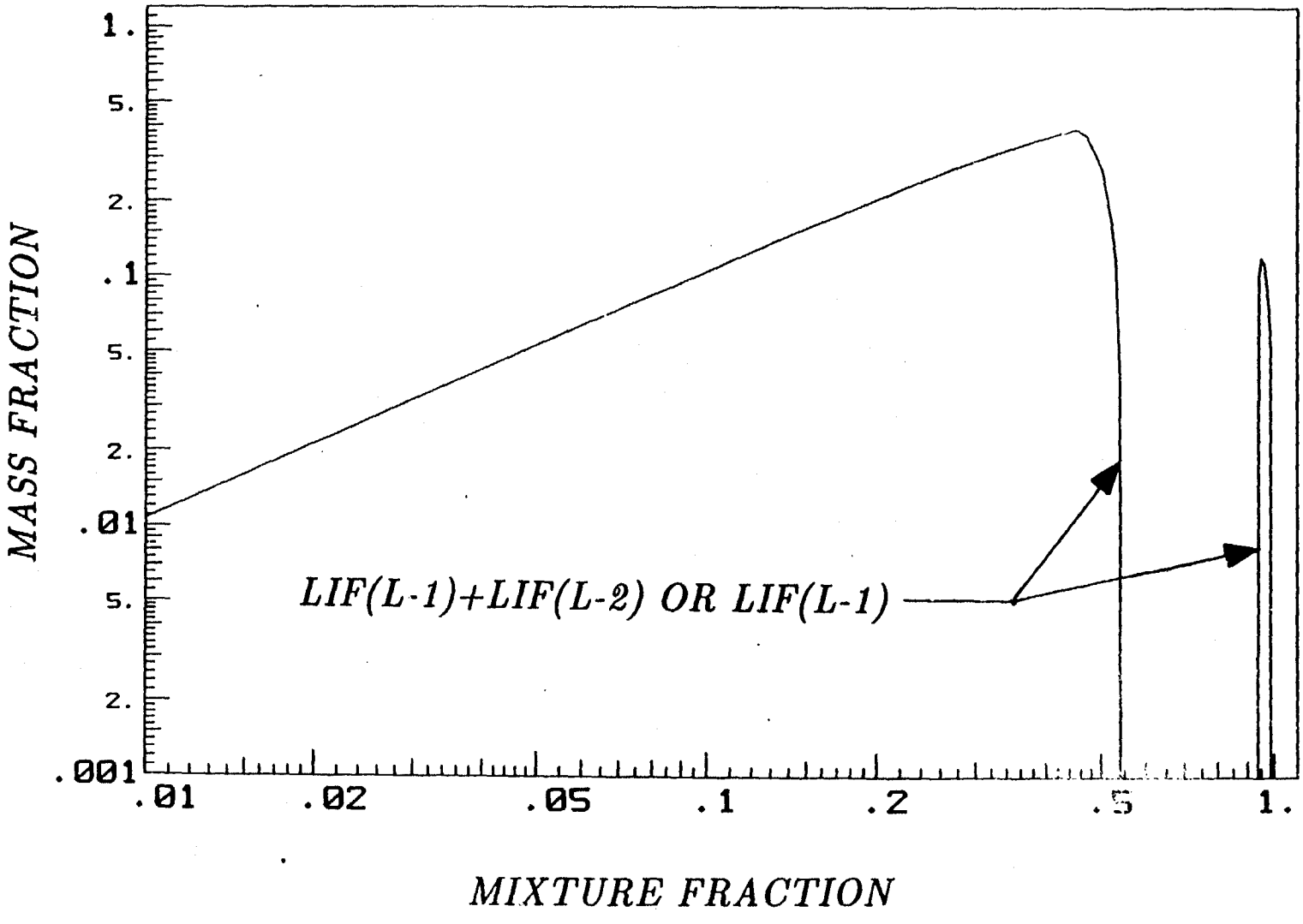

Fig.30 Equilibrium Compositions of $Li - SF_6$ System with Li at 1586 K and SF_6 Gas at 298 K

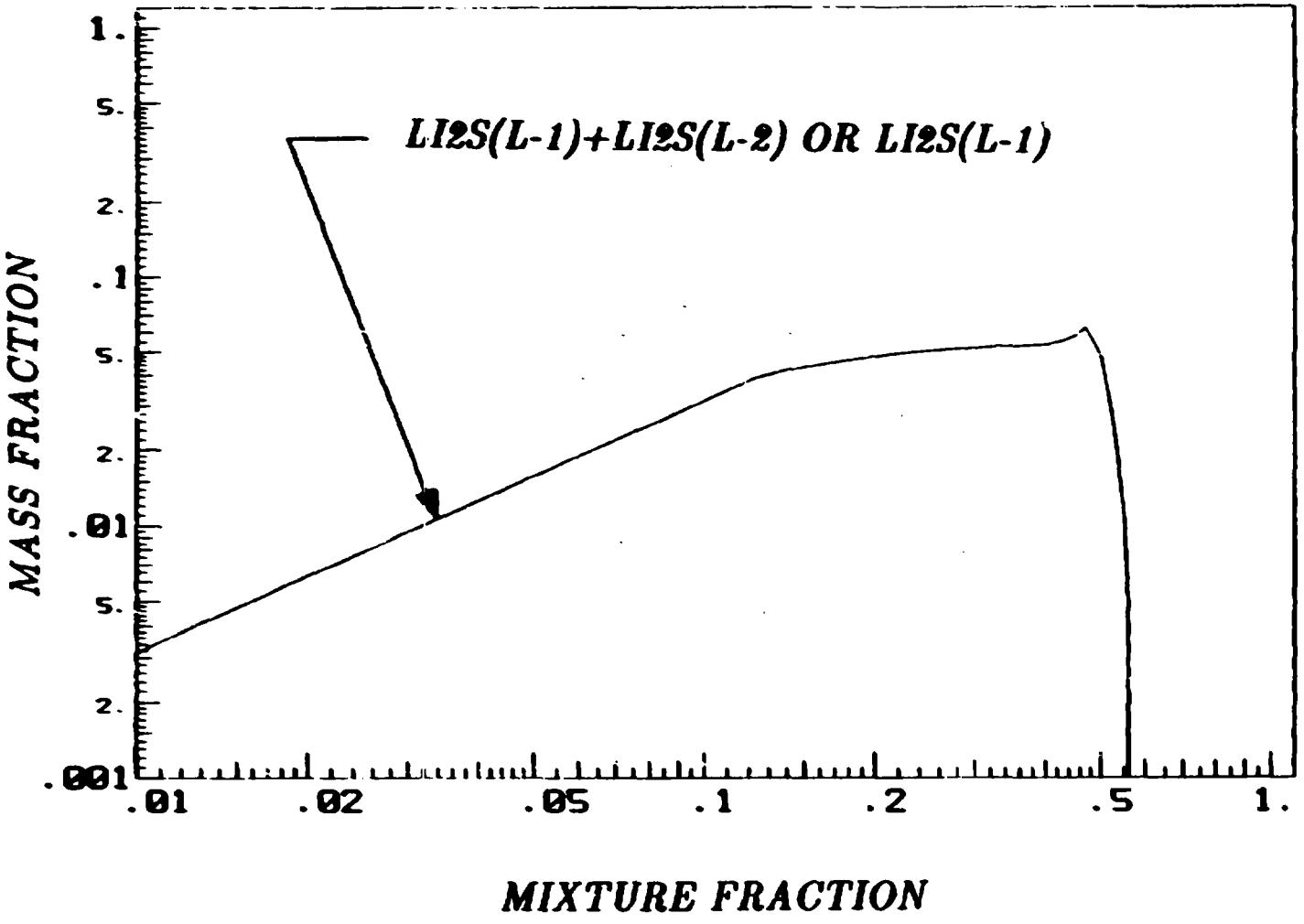

Fig.31 Equilibrium Compositions of $Li - SF_6$ System with Li at 1130 K and SF_6 Gas at 298 K

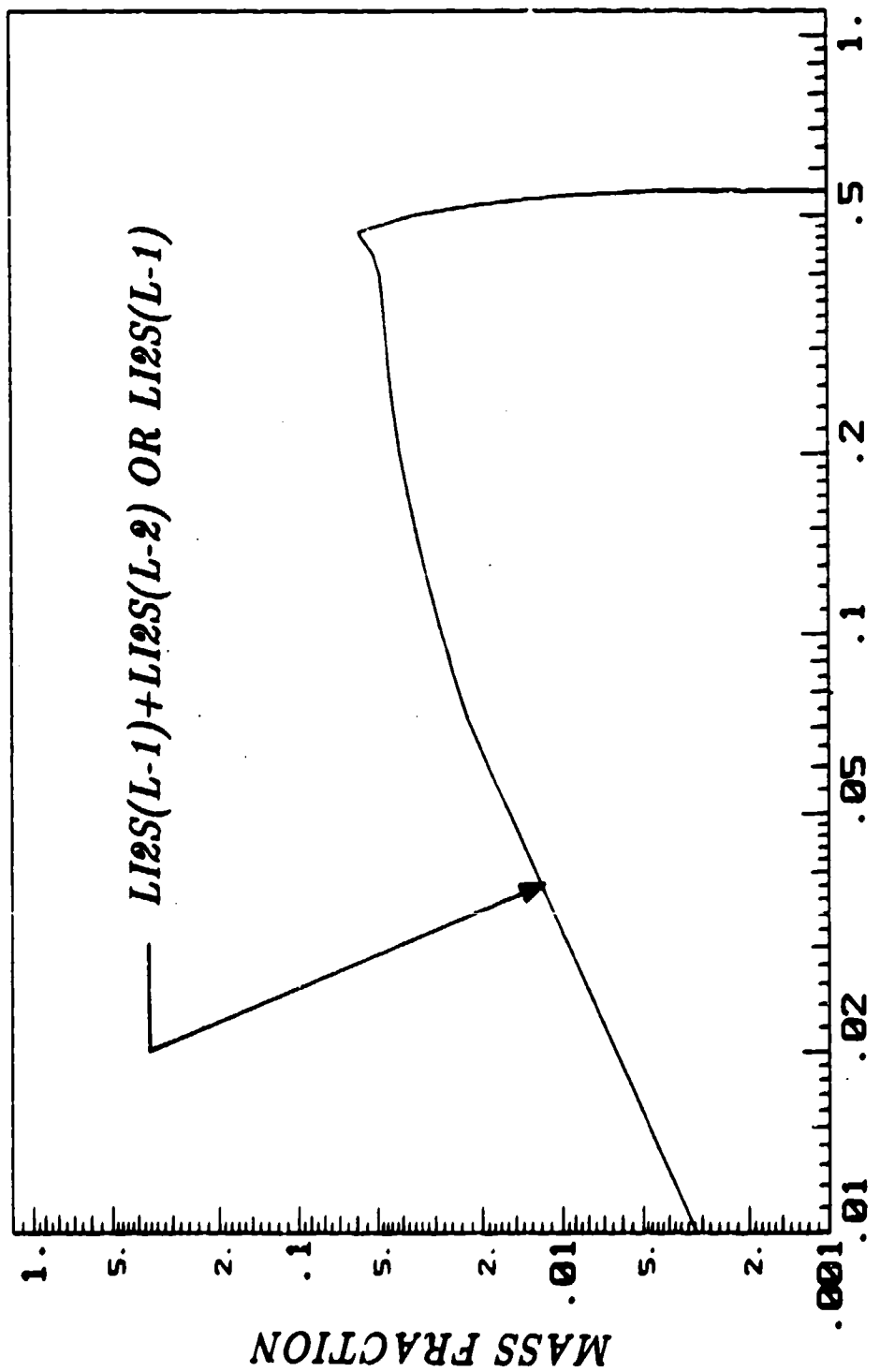

Fig.32 Equilibrium Compositions of $Li - SF_6$ System with Li at 1358 K and SF_6 Gas at 298 K

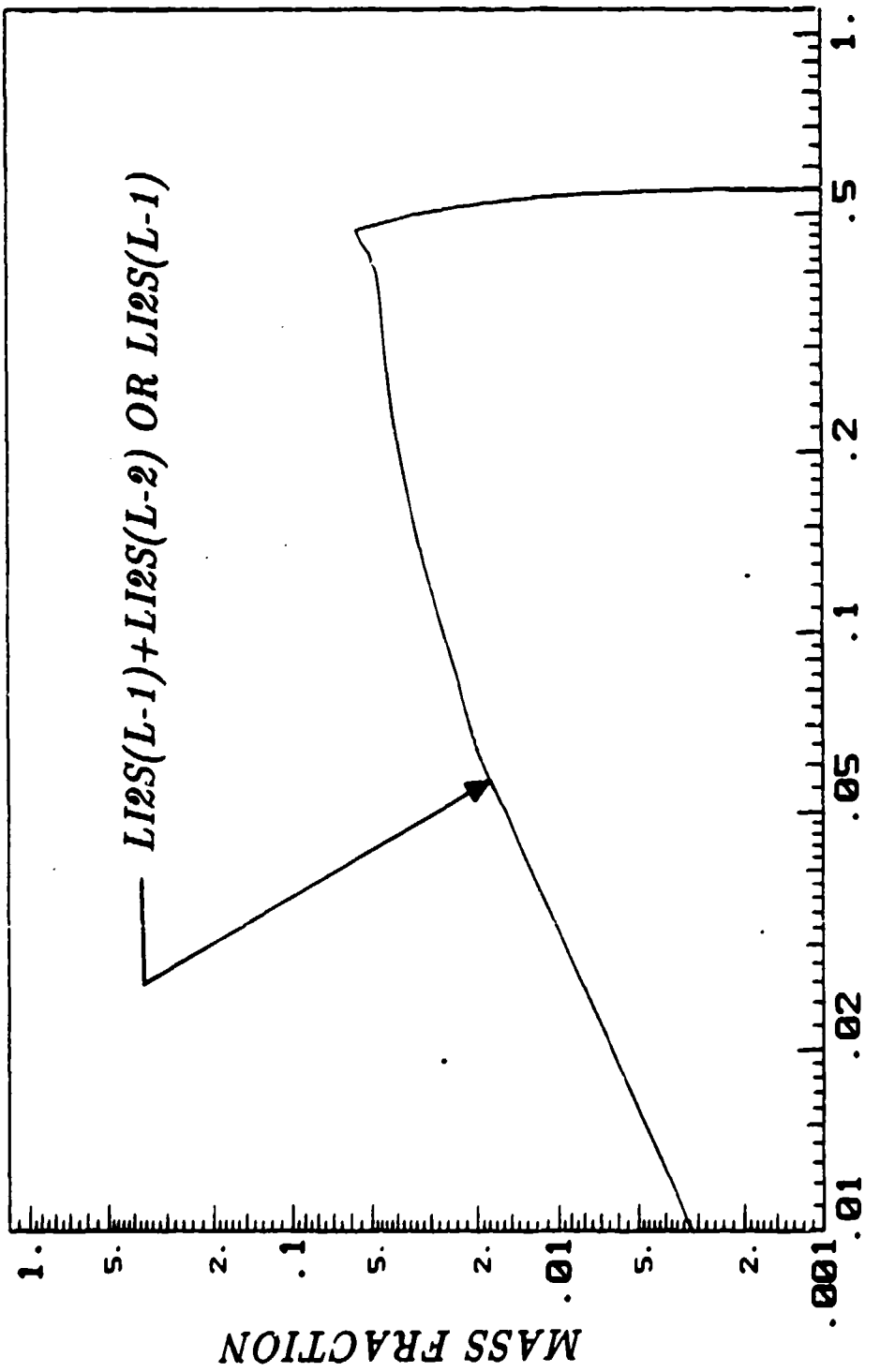

Fig.33 Equilibrium Compositions of $Li - SF_6$ System with Li at 1415 K and SF_6 Gas at 298 K

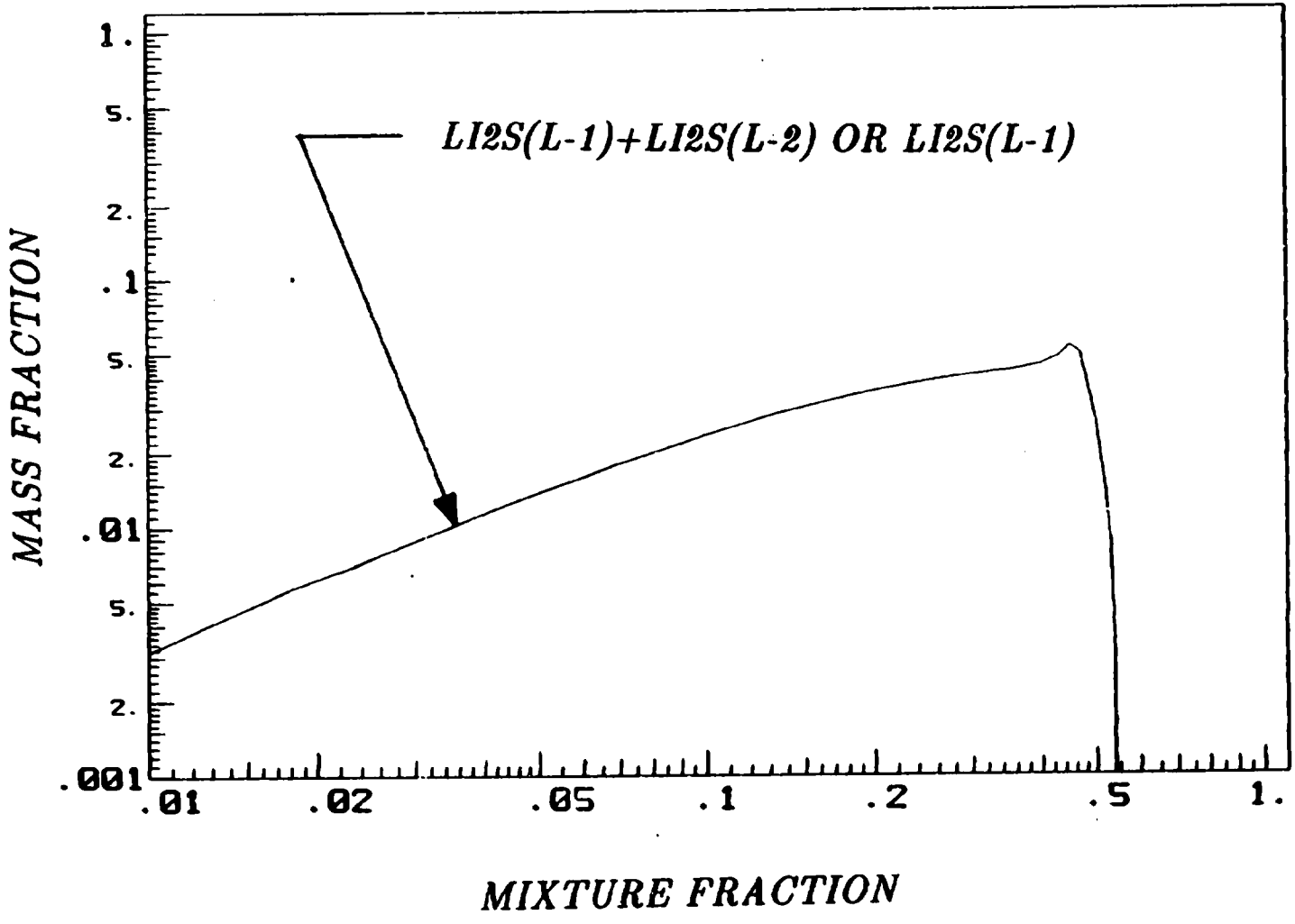

Fig.34 Equilibrium Compositions of $Li - SF_6$ System with Li at 1586 K and SF_6 Gas at 298 K

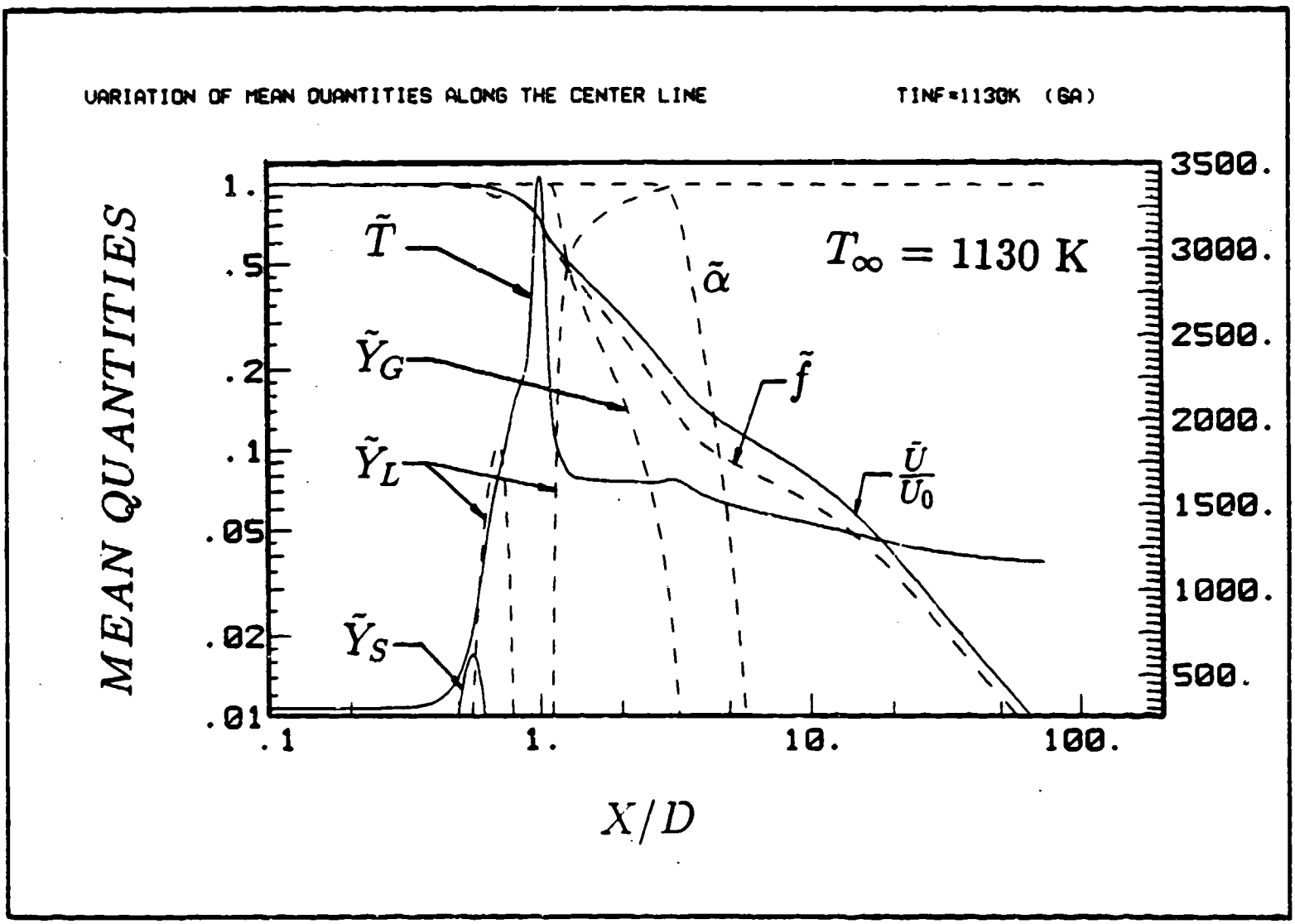

Fig.35 Predicted Mean Quantities Along The Jet Axis

SF_6 Gas (298K) Discharged In Molten Li (1130K)

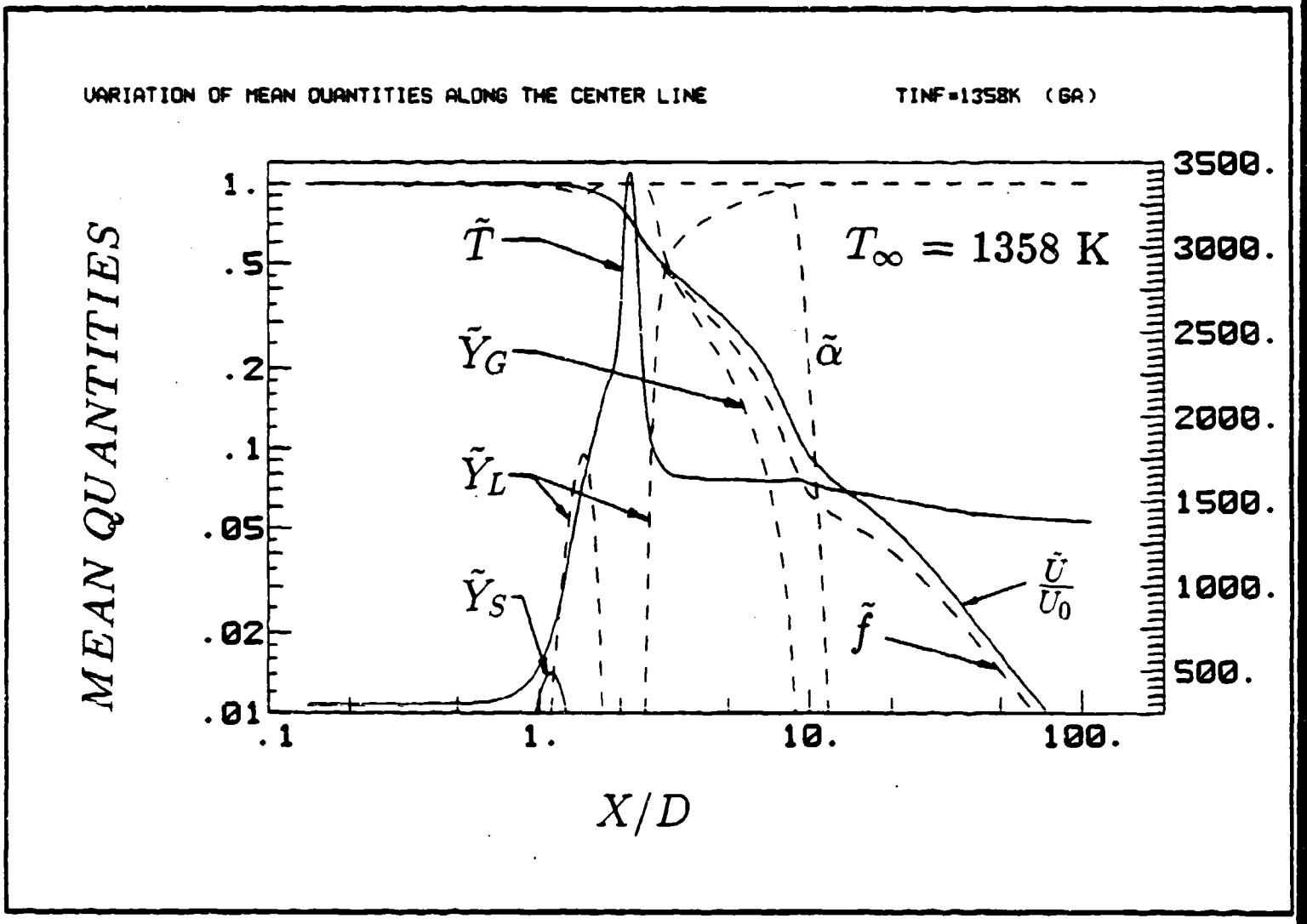

Fig.36 Predicted Mean Quantities Along The Jet Axis

SF_6 Gas (298K) Discharged In Molten Li (1358K)

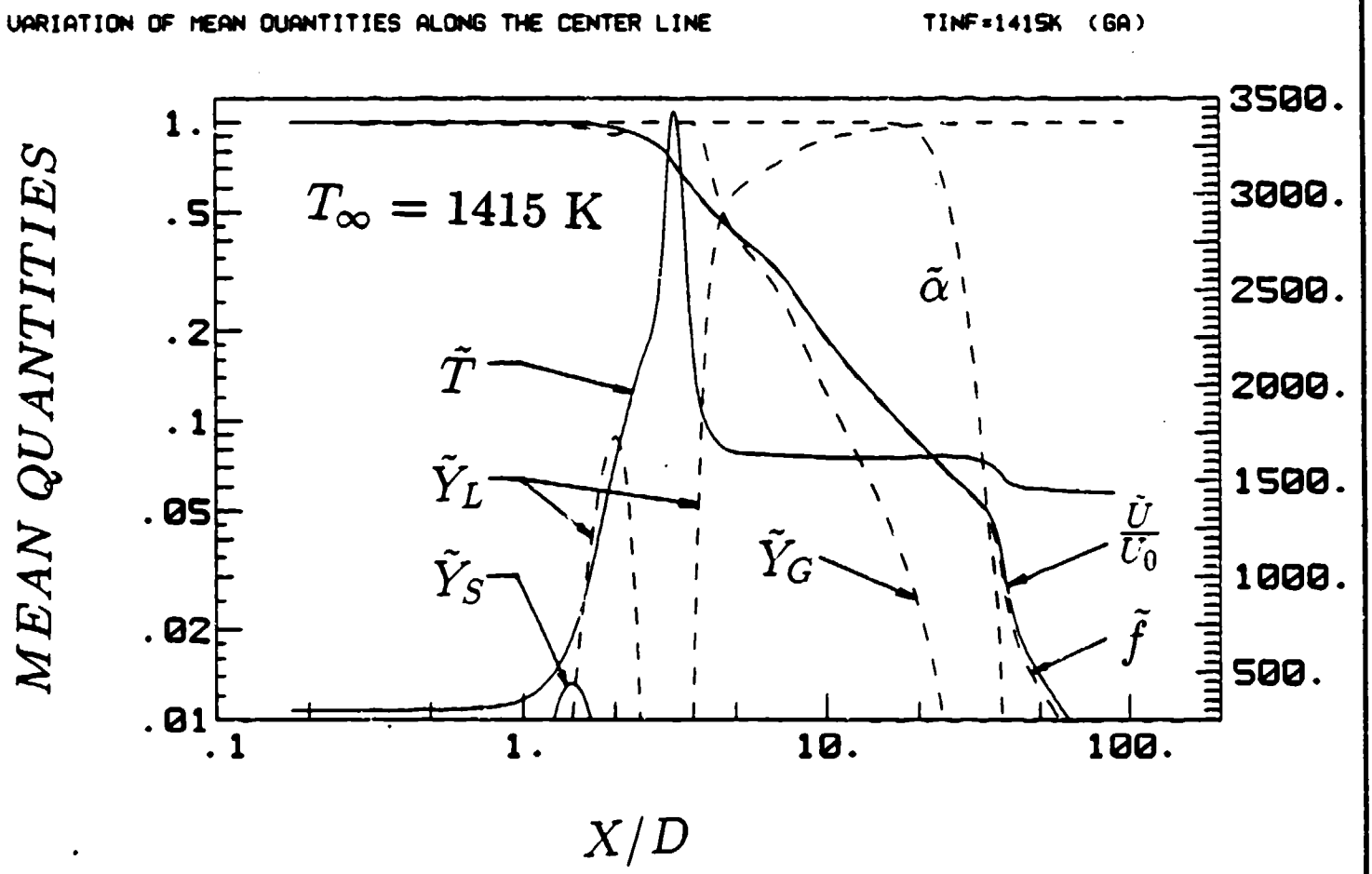

Fig.37 Predicted Mean Quantities Along The Jet Axis

SF_6 Gas (298K) Discharged In Molten Li (1415K)

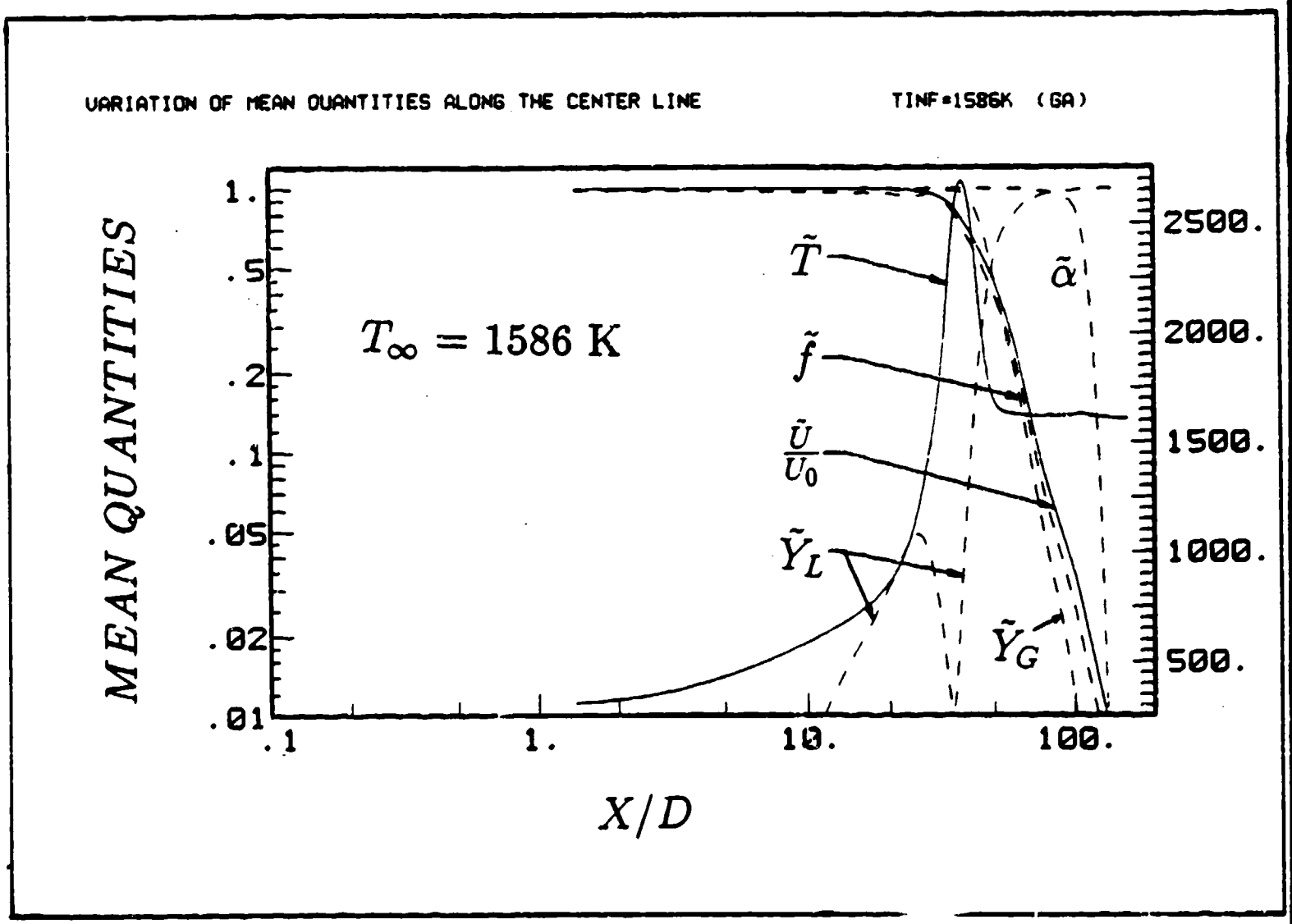

Fig.38 Predicted Mean Quantities Along The Jet Axis

SF_6 Gas (298K) Discharged In Molten Li (1586K)

APPENDIX A. Equilibrium Computer Program And Results For $Li - SF_6$ Reaction

APPENDIX B. Flow Structure Computer Program And Results For $Li - SF_6$ Reaction

Legible copy can not be reproduced.

Interested readers should contact the author (S.H.Chan).

ONR REPORT DISTRIBUTION LIST CLOSED,
LIQUID METAL COMBUSTION*

Dr. Gabriel D. Roy (2)
Mechanics Division, Code 1132 P
Office of Naval Research
800 N. Quincy Street
Arlington, VA 22217-5000

Dr. Richard S. Miller (2)
Mechanics Division, Code 1132P
Office of Naval Research
800 N. Quincy Street
Arlington, VA 22217-5000

Dr. Lynn A. Parnell
Naval Ocean System Center
Code 6341
San Diego, CA 92152-5000

Defense Documentation Center (12)
Building 5, Cameron Station
Alexandria, VA 22314

Technical Information Division (6)
Naval Research Laboratory
4555 Overlook Avenue SW
Washington, DC 20375

Dr. Robert Nowark
Chemistry Division
Office of Naval Research
800 N. Quincy Street
Arlington, VA 22217

Dr. Albert D. Wood
Technology Programs
Office of Naval Research
800 N. Quincy Street
Arlington, VA 22217

Dr. H. W. Carhart
Combustion and Fuels
Naval Research Laboratory
Washington, DC 20375

Professor Allen Fuhs
Department of Aeronautics
Naval Post Graduate School
Monterey, CA 93943

Division Director
Engineering and Weapons
US Naval Academy
Annapolis, MD 21402

Mr. Francis J. Ramano
Code 63R3
Naval Sea Systems Command
Washington, DC 20363

Dr. Jerry A. Smith
Chemistry Division
Office of Naval Research
800 N. Quincy Street
Arlington, VA 22217

Mr. Robert Tompkins
Code 36621, Bldg. 126T
Naval Underwater System Center
Newport, RI 02841

Mr. Maurice F. Murphy
Code R33, Room 4-1711
Naval Surface Weapons, White Oak
Silver Spring, MD 20910

Dr. Kurt Mueller
Code R10
Energetic Materials Division
Naval Surface Weapons Center,
White Oak
Silver Spring, MD 20910

Dr. Earl Quandt, Jr.
Code 2704
David Taylor Naval Ship
Research and Development Center
Annapolis, MD 21402

---

*One copy except as noted in parenthesis.

Mr. Richard Bloomquist
Code 2752
David Taylor Naval Ship
Research and Development Center
Annapolis, MD 21402

Dr. Lawrence P. Cook
High Temperature Processes Group
National Bureau of Standards
Washington, DC 20234

Professor A. Murty Kanury
Department of Mechanical Engineering
Oregon State University
Corvallis, OR 97331

Professor Irvin Glassman
Department of Mechanical and
Aerospace Engineering
Engineering Quadrangle
Princeton University
Princeton, NY 08544

Dr. W. Lee
Research and Technology Department
Naval Surface Weapons Center
Silver Springs, MD 20703

Professor Norman Chigier
Department of Mechanical Engineering
Carnegie-Mellon University
Pittsburgh, PA 15213

Professor George Janz
Cogswell Laboratory, R306
Department of Chemistry
Rensselaer Polytechnic Institute
Troy, NY 12181

Dr. Leonard Leibowitz
Chemical Technology Division
Argonne National Laboratory
9700 South Cass Avenue
Argonne, IL 60439

Professor John Tarbell
104 Fenske Laboratory
Pennsylvania State University
University Park, PA 16801

Professor Thomas E. Daubert
104 Fenske Laboratory
Pennsylvania State University
University Park, PA 16801

Dr. J. Braunstein
Research Division
Oak Ridge Operations
Department E
Oak Ridge, TN 37831

Dr. Hugh H. Darsie
Advanced Technology Group
Sundstrand Energy Systems
4747 Harrison Avenue
Rockford, IL 61101

Professor Gerard M. Faeth
Department of Aerospace
Engineering
University of Michigan
Ann Arbor, MI 48109

Mr. Ron Kessing
MS 1207-4P
Fluid System Division
Allied Signal Corp.
1300 West Warner Rd.
P.O. Box 22200
Tempe, AZ 85285

Dr. Daniel H. Kiely
Power and Energy Group
Pennsylvania State University
Applied Research Laboratory
P.O. Box 30
State College, PA 16801

Professor Darryl E. Metzger
Department of Mechanical
and Aerospace Engineering
Arizona State University
Tempe, AZ 85281

Professor George A. Brown
Department of Mechanical Engineering
and Applied Mechanics
University of Rhode Island
Kingston, RI 02881

Professor Paul E. Dimontakis
Mail Code 301-46
Graduate Aeronautical Laboratory
California Institute of Technology
Pasadena, CA 91125

Dr. Charles H. Berman
Aerochem Research Laboratories, Inc.
P.O. Box 12
Princeton, NJ 08542

Dr. Donald M. McEligot
Westinghous Naval System Division
62 Johnny Cake Hill
Middletown, RI 02840

Dr. C. William Kauffman
Department of Aerospace Engineering
The University of Michigan
Ann Arbor, MI 48109-2140

Professor Lea D. Chen
Department of Mechanical Engineering
The University of Iowa
Iowa City, IA 5542

LCDR Mike Barry
NISC - 4311
Naval Intelligence Support Center
4301 Suitland Road
Washington, DC 20390

Dr. Raafat H. Guirguis
Laboratory for Computational
Physics
Code 4040
Naval Research Laboratory
Washington, DC 20375

Professor John Cimbala
157 Hammond Bldg.
Department of Mechanical Engrg.
Pennysylvania State University
University Park, PA 16802

Mr. David White
Manager of Advanced Development
Solar Turbine Inc.
2200 Pacific Highway
P.O. Box 85376
San Diego, CA 92138-5376

Mr. William J. Greenlee
Engineering Manager Research
Department 741A6, Sundstrand ATG
4747 Harrison Avenue
P.O. Box 7002
Rockford, IL 61125-7002